Journal of Neuroinflammation

RESEARCH Open Access

Glutamine metabolism modulates microglial NLRP3 inflammasome activity through mitophagy in Alzheimer's disease

Zhixin Zhang[1,2], Miao Li[1], Xiang Li[1], Zhiyang Feng[1], Gan Luo[1], Ying Wang[1] and Xiaoyan Gao[1*]

Abstract
The NLR family pyrin domain containing 3 (NLRP3) inflammasome in microglia is intimately linked to the pathogenesis of Alzheimer's disease (AD). Although NLRP3 inflammasome activity is regulated by cellular metabolism, the underlying mechanism remains elusive. Here, we found that under the pathological conditions of AD, the activation of NLRP3 inflammasome in microglia is accompanied by increased glutamine metabolism. Suppression of glutaminase, the rate limiting enzyme in glutamine metabolism, attenuated the NLRP3 inflammasome activation both in the microglia of AD mice and cultured inflammatory microglia. Mechanistically, inhibiting glutaminase blocked the anaplerotic flux of glutamine to the tricarboxylic acid cycle and amino acid synthesis, down-regulated mTORC1 signaling by phosphorylating AMPK, which stimulated mitophagy and limited the accumulation of intracellular reactive oxygen species, ultimately prevented the activation of NLRP3 inflammasomes in activated microglia during AD. Taken together, our findings suggest that glutamine metabolism regulates the activation of NLRP3 inflammasome through mitophagy in microglia, thus providing a potential therapeutic target for AD treatment.

Keywords Alzheimer's disease, Microglia, NLRP3 inflammasome, Glutamine metabolism, Mitophagy

Introduction

Alzheimer's disease (AD) is a typical progressive neurodegenerative disease characterized by microglia-mediated neuroinflammation that is central to its pathology [1, 2]. Increasing evidence demonstrated that amyloid-β (Aβ)-induced activation of NLR family pyrin domain containing 3 (NLRP3) inflammasomes in microglia is essential for the maturation of interleukin-1β (IL-1β) and the subsequent development of neuroinflammation [3, 4]. In the brains of AD patients or AD animal models, NLRP3 inflammasome activation is significantly increased, while mice with NLRP3 knockout largely display alleviation of AD-associated symptoms such as neuroinflammation and impaired spatial memory, among others [5–7]. This connection suggests that the NLRP3 inflammasome is a potential therapeutic target for controlling neuroinflammation in AD. However, although the phenotype and functional characteristics of NLRP3 inflammasomes are well known, the molecular mechanism responsible for its activity regulation during AD has thus far remained elusive.

Activation of the NLRP3 inflammasome gives rise to mature caspase-1, resulting in subsequent cleavage of pro-IL-1β, pro-IL-18, and gasdermin D into their active forms, which then exert immunomodulatory effects

*Correspondence:
Xiaoyan Gao
gaoxiaoyan@bucm.edu.cn
[1]School of Chinese Materia Medica, Beijing University of Chinese Medicine, Beijing 102488, China
[2]Institute of Pharmacy, Shandong University of Traditional Chinese Medicine, Jinan 250355, China

[8–10]. Some studies have shown that the reactive oxygen species (ROS) and mitochondrial DNA (mtDNA) released by dysfunctional mitochondria will activate NLRP3 inflammasome, and enhancing mitophagy can effectively inhibit the activation of NLRP3 inflammasome by scavenging dysfunctional mitochondria [11–13]. Mitochondria play a key role in the cellular metabolic network. Tricarboxylic acid cycle (TCA), oxidative phosphorylation, fatty acid oxidation, nucleotide synthesis, amino acid metabolism and so on all occur in mitochondria [14]. Studies have found that metabolic reprogramming occurs in activated microglia of AD [15–17]. Therefore, we speculate that this metabolic disturbance will inevitably affect the function of mitochondria. Furthermore, it has been previously shown that NLRP3 inflammasome activation is also associated with disruption of metabolic pathways, including TCA metabolism [18, 19], fatty acids [20, 21], cholesterol [22, 23], and glycolysis [24, 25]. Based on the above background, we propose a conjecture: whether metabolic disturbance in the activated microglia of AD affects the activity of NLRP3 inflammasome by regulating mitochondrial function.

Glutamine is the most abundant nonessential amino acid in most mammals [26]. In rapidly proliferating cells such as cancer cells or activated immune cells, glutamine metabolism initiated by glutaminase can replenish the TCA cycle to generate reducing equivalents that drive the mitochondrial respiratory chain and produce precursors for lipid and protein biosynthesis [27, 28]. Glutamine anaplerosis can lead to increased succinate production, the accumulation of which can trigger a series of events that cumulatively result in heightened release of the pro-inflammatory cytokine IL-1β in mouse macrophages [29]. Thus, we speculate that glutamine metabolism may affect the activity of NLRP3 inflammasome. However, whether glutamine metabolism in microglia is disturbed under pathological conditions of AD, and the effects of glutamine metabolism on NLRP3 inflammasome-dependent secretion of IL-1β have not been reported.

Here, data from metabolomics and metabolic flux analysis show that under pathological conditions of AD, glutamine metabolism is markedly increased in the microglia of 8-month-old female APPswe/PSEN1dE9 transgenic (APP/PS1) mice and in cultured inflammatory primary microglia induced by Aβ, accompanied by NLRP3 inflammasome activation and secretion of active IL-1β. While inhibiting glutamine metabolism by depletion or silencing of glutaminase 1 isoform (GLS1) can hinder the anaplerotic flux of glutamine to the TCA cycle, consequently limiting amino acid synthesis and inducing mitophagy in microglia. The promotion of mitophagy can reduce intracellular ROS, ultimately inhibiting NLRP3 inflammasome activation and production of IL-1β. These findings suggest that glutamine metabolism may be a determining regulatory factor in the activation of NLRP3 inflammasomes in microglia and point to glutamine metabolism as a promising therapeutic target for treating AD.

Materials and methods

Animals

All mice used were in C57BL/6 background. 8-month-old female Alzheimer's disease transgenic mice (APP/PS1) and wild-type (WT) littermates were provided by Nanjing Biomedical Research Institute of Nanjing University (Nanjing, China). All mice were housed under standard conditions in a specific pathogen-free facility monitoring health status, with temperature of 20–24℃, humidity of 40–70%, 12 h light-dark cycle, and free access to food and water. Animal care and handling was performed according to the declaration of Helsinki and approved by the ethical committees of Beijing University of Chinese Medicine.

Primary microglia culture

Primary microglia were isolated from the cerebral cortices of male and female C57BL/6 mice within 24 h of birth. Meninges on the cerebral cortices were carefully peeled off in ice-cold D-Hank's solution (Solarbio). All cerebral cortices were cut into small pieces with scissors and transferred to a centrifuge tube containing 0.125% trypsin solution (Gibco) for 10 min at 37℃. After centrifugation, Dulbecco's modified Eagle's medium (DMEM; Gibco) containing 1% penicillin-streptomycin (P/S; Sigma-Aldrich) and 10% fetal bovine serum (FBS; Gibco) was added to the sediment. Resuspend the cells and use 70 μm cell screen for filtration. Then, the cells were plated on T-25 cell culture flasks which pre coated with poly-L-Lysine (PLL; Sigma-Aldrich) at 5.0×10^5 cells/ml, and 4 ml culture medium (DMEM with 1% P/S and 10% FBS) was added to each bottle (37℃, 5% CO_2). Half of the culture medium was renewed every three days. On day 10, microglia were isolated from mixed glial cells by tapping the flask. The isolated microglia were plated on 24-well cell culture plates which pre coated with PLL at 2.0×10^5 cells/ml and incubated for 3 d before using.

Animal treatments

For inhibition of GLS1 expression and its initiated glutamine metabolism, APP/PS1 mice were treated with telaglenastat (CB-839) (50 mg/kg, administered by oral gavage once a day for 1 week; Sigma-Aldrich). Vehicle for CB-839 was corn oil.

Isolation of microglia from adult mouse brains

The microglia were isolated from the brain of 8-month-old female APP/PS1 mice or WT mice. In brief, mice were anesthetized with isoflurane (Sigma-Aldrich) and

transcardially perfused with ice-cold saline, and then the brain (excluding the cerebellum and olfactory bulbs) was dissected. Meninges on the brain were carefully peeled off in ice-cold D-Hank's solution (Solarbio). The tissue were cut into small pieces with scissors and transferred to a centrifuge tube containing 100 U Papain (Worthington), 6 U Dispase II (Sigma-Aldrich) and 100 U DNase I (Sigma-Aldrich) for 30 min at 37℃. After centrifugation, resuspend the cells and use 70 μm cell screen for filtration. Microglia were isolated from the single-cell suspension of mouse brain using CD11b MicroBeads (130-093-634, Miltenyi Biotec) and a magnetic-activated cell sorting (Miltenyi Biotec) Separator.

Flow cytometry

The isolated microglia from the brain of 8-month-old female APP/PS1 mice or WT mice were stained with Zombie-NIR fixable viability dye (423106, Biolegend) for 30 min at room temperature to exclude the dead cells, and then stained with Brilliant Violet 421 anti-CD11b (101236, Biolegend). Fixation/Permeabilization Solution Kit (BD Biosciences) was used for intracellular staining according to manufacturer's instructions, and the cells were stained with FITC-conjugated anti-IL-1β (508206, Biolegend), or FLICA 660 Caspase-1 reagent (ICT-9122, Biomol) for 30 min at room temperature and processed to flow cytometry analysis. A FACSCanto II cytometer (BD Biosciences) was used for all flow cytometric assays, data were acquired and analyzed by a FACSDIVA software (BD Biosciences) or FlowJo™ v10 software.

Preparation of Aβ1−42

1 mg $A\beta_{1-42}$ peptides (Sigma-Aldrich) were dissolved in 1 ml 1,1,1,3,3,3-hexafluoro-2-propanol (HFIP; Sigma-Aldrich) and sonicated for 10 min in an ice-bath, followed by incubation with shaking at 4 °C for 3 h. The HFIP in resulting solution was evaporated under a gentle stream of N_2 gas to obtain $A\beta_{1-42}$ films. Dissolving $A\beta_{1-42}$ peptide films to 2 mM in 110.8 μl dimethyl sulfoxide (DMSO; Sigma-Aldrich) and diluting the solution to 5 μM in DMEM. Then incubated the resulting solution at 37℃ for 0 h (monomeric $A\beta_{1-42}$), 24 h (oligomeric $A\beta_{1-42}$, $oA\beta_{1-42}$) and 96 h (fibrillary $A\beta_{1-42}$).

Stimulation of primary microglia

Primary microglia which isolated from the cerebral cortices of male and female C57BL/6 mice within 24 h of birth were plated in 24-well cell culture plates 3 d before using. Cells were treated with lipopolysaccharide (LPS) from *Escherichia coli* (100 ng/ml; Sigma-Aldrich) for 6 h. Medium was removed and replaced with $oA\beta_{1-42}$ (5 μM) for 12 h or ATP (5 mM; Sigma-Aldrich) for 4 h to activate the NLRP3 inflammasome. In order to activate the AIM2 inflammasome, LPS-primed microglia were treated with poly(dA: dT) (2 μg/ml; Invivogen) for 6 h. In order to activate the NLRC4 inflammasome, LPS-primed microglia were treated with flagellin from *Salmonella typhimurium* (10 μM; Invivogen) for 2 h. In order to activate the NLRP1 inflammasome, LPS-primed microglia were treated with muramyl dipeptide (MDP) (200 ng/ml; Invivogen) for 6 h. In some experiments, primary microglia were pre-incubated with 10 μM bis-2-(5-phenylacetamido-1,3,4-thiadiazol-2-yl)ethyl sulfide (BPTES; Sigma-Aldrich) 4 h to inhibit GLS1 expression, or N-acetylcysteine (NAC; 100 μM, 4 h; Sigma-Aldrich) to clear ROS, or nicotinamide mononucleotide (NMN; 100 μM, 4 h; Sigma-Aldrich) to promote mitophagy, or rapamycin (10 nM, 4 h; Sigma-Aldrich) to block the mTORC1 pathway. Then, LPS (100 ng/ml, 6 h) and $oA\beta_{1-42}$ (5 μM, 12 h) were added sequentially.

Tissue processing

For immunohistochemistry, the 8-month-old female APP/PS1 mice or WT mice ($n=3$ per group) were anesthetized with isoflurane (Sigma-Aldrich) and transcardially perfused with ice-cold saline followed by ice-cold 10% neutral-buffered formalin (Thermo Fisher Scientific) and brains were dissected and post-fixed in 10% neutral-buffered formalin before using. Brains were embedded in paraffin and sectioned at 4 μm.

For ELISA ($n=6$ per group), the brains were dissected from anesthetized mice and isolate the hippocampus were isolated on ice, then immediately stored −80℃ before using. The ice-cold PBS solution was added to the hippocampus in the ratio of 2.5 μl/mg, and the soluble components were extracted on ice using a tissue homogenizer (OMNI International). Samples were centrifuged (14,000 × g, 4 °C, 10 min) and the supernatant recovered.

Immunohistological staining

Immunohistochemical staining was prepared by tissue sections of the whole brain which embedded with paraffin. After deparaffinization and rehydration through graded alcohols, citrate buffer was used for antigen retrieval at 90°C for 10 min. After gradually cooled to block endogenous peroxidase activity at room temperature, the sections were then washed with PBS and blocked with goat serum for 30 min at 37°C. Removed the goat serum, and incubated the sections with mouse-anti Iba-1 (1:10000; ab283319, Abcam) or mouse-anti Aβ antibody (5 μg/ml; ab126649, Abcam) at 4°C for 12 h. Rewarming the sections at room temperature for 30 min and intubated with biotin-labelled goat anti-mouse secondary antibody (1:500; ab47827, Abcam) and streptomycin anti-biotin peroxidase for 10 min each. Then, labelled the sections with 3,3'-diaminobenzidine, followed by hematoxylin counterstaining. Finally, the

sections were washed with PBS and dehydrated by gradients of ethanol and xylene.

ELISA assays

Cell culture supernatants and mouse hippocampus were examined for IL-1β (KE10003, Proteintech), IL-18 (KE00025, Proteintech), $A\beta_{1-42}$ (E03A0039, Bluegene) and total soluble Aβ (E03A0050, Bluegene) with ELISA kits according to the manufacturer's instructions.

Western blotting

The supernatants of protein lysates of cells or tissues were harvested using RIPA buffer (1 mM PMSF, 10 μl/ml of Proteases Inhibitors Cocktail; Gibco) and PBS was added to the final concentration of 4 mg/ml, and then added 5× SDS loading buffer (Beyotime) in the ratio of 4:1 according to the volume, and then vortex mixing. Boiled the samples at 95–100 °C for 5 min and the protein concentration were quantified with a Pierce Bicinchoninic Acid (BCA) Protein Assay kit (Beyotime) according to manufactory instructions. To concentrate the protein from the cell culture supernatant, 20 μL Strataclean Resin (Agilent) was added to 1 mL of supernatant and then vortexed for 2 min. The mixture was centrifuged at 2000 × g for 2 min at room temperature, after which the supernatant was removed and discarded. 40 μL RIPA buffer (Gibco) was added to the remaining pellet and the protein concentration was determined by BCA Protein Assay Kit (Beyotime). Loading the samples into a 5% stacking gel and 8-12% resolving gel. Proteins were resolved using a Bio-Rad gel running system and the electrophoretic transfer of proteins onto PVDF membrane was performed using a Bio-Rad wet transfer system. After transfer, the membrane was washed with TBST and then incubated in non-fat milk powder (5% in TBST) rolling 2 h at room temperature. Washed with TBST three times for 10 min each time. Then, the membrane was incubated in primary antibody (diluted in 5% milk powder): rabbit polyclonal anti-IL-1β (1:1000; 16806-1-AP, Proteintech), rabbit polyclonal anti-caspase-1 (1:1000; 22915-1-AP, Proteintech), rabbit polyclonal anti-NLRP3 (1:500; 19771-1-AP, Proteintech), goat polyclonal anti-ASC (1:500; ab175449, Abcam), rabbit polyclonal anti-GSDMD (1:1000; 20770-1-AP, Proteintech), mouse monoclonal anti-m-aconitase (1:1000; ab110321, Abcam), rabbit polyclonal anti-PINK (1:1000; 23274-1-AP, Proteintech), mouse monoclonal anti-parkin (1:1000; ab77924, Abcam), rabbit polyclonal anti-p62 (1:1000; 18420-1-AP, Proteintech), rabbit polyclonal anti-LC3 (1:1000; 18725-1-AP, Proteintech), rabbit polyclonal anti-Raptor (1:1000; 20984-1-AP, Proteintech), rabbit polyclonal anti-AMPKα (1:1000; 66536-1-Ig, Proteintech), rabbit monoclonal anti-p-AMPKα (Thr172) (1:1000; ab133448, Abcam), rabbit polyclonal anti-KGA/GAC (1:1000; 12855-1-AP, Proteintech), mouse monoclonal anti-GAPDH (1:10000; 60004-1-Ig, Proteintech) or mouse monoclonal anti-β-actin (1:10000; 66009-1-Ig, Proteintech) overnight at 4 °C. Washed with TBST three times for 10 min each time. Incubated the membrane with secondary antibody for 2 h at room temperature. Washed with TBST three times for 10 min each time. Immersed the membrane in WesternBright ECL Spray (BioRad) prior to visualization for 1–5 min. A ChemiDoc™ MP Imaging System (Bio-Rad) was used for protein visualization and Image Lab Software (Bio-Rad) was used for the quantification of western blot images.

LDH release assay

Cell culture supernatants were collected after corresponding treatments and the LDH release was detected using the LDH cytotoxicity assay kit (Beyotime). Briefly, 60 μL of LDH detection reagents was added into 120 μL supernatants in each well of 96-well plate. Mixed well and incubated at room temperature in the dark for 30 min. Then, the absorbance was measured at 490 nm using a FLUOstar optima.

Metabolomics analysis

Cells were lysed in -80℃ methanol/water (50/50, v) on ice and samples were centrifuged (14,000 × g, 4 °C, 10 min) and the supernatant recovered. Then, samples were blow dry with nitrogen and resuspended in 50 μl methanol/water (50/50, v). The separation of the metabolites was performed on a ThermoFisher Q-Exactive Orbitrap mass spectrometer equipped with ACQUITY UPLC BEH Amide column (100×2.1 mm, 1.7 μm; Waters). The gradient mobile phase was a mixture of acetonitrile/water (95/5, v) containing 0.1% ammonium acetate (A) and water containing 0.1% ammonium formate (B), and gradient elution was programmed as follows: 0–1 min, 5% B; 1–7 min, 5-50% B; 7–9 min, 50% B; 9–9.1 min, 50%-5% B; 9.1–12 min, 5%B; flow rate: 0.3 ml/min. The analytical column and autosampler temperatures were maintained at 45 °C and 4 °C, respectively. The injection volume was set at 5 μl and the metabolites were monitored in full-scan/dd-MS^2 mode (positive mode at a range of *m/z* 50-1500). Data were imported to the Progenesis QI (Waters Corp., Milford, USA) for peak alignment to obtain a three-dimensional data list containing the retention time, *m/z*, and peak intensity of each sample. The Metaboanalyst 5.0 database (www.metaboanalyst.ca) was used for the hierarchical clustering, partial least squares discriminant analysis and variable importance in projection analysis. Human metabolome database (HMDB, www.hmdb.ca) and the Kyoto Encyclopedia of Genes and Genomes (KEGG) Compound database (www.genome.jp/kegg) were used for putative metabolite identification based on the monoisotopic molecular weight and MS/MS spectrum.

Oxygen consumption rate (OCR) measurements

The OCR was measured using an XF96 extracellular analyser (Seahorse Bioscience). Primary microglia were plated in an XF96 cell culture plates at a density of 10,000 cells/well. After incubation for 3 d, the cells were treated with LPS (100 ng/ml; Sigma-Aldrich) for 6 h. The medium was removed and replaced with oAβ_{1-42} (5 μM) for 12 h to activate the NLRP3 inflammasome. Right before the assays, the media were then removed and these cells were changed to XF Seahorse DMEM medium (Seahorse Bioscience) at pH 7.4 supplemented with 2 mM glutamine, 10 mM glucose and 2 mM sodium pyruvate and incubated for 1 h at 37℃ without CO_2. The OCR was measured at the basal state and after sequential injection of 1 μM oligomycin, 1 μM carbonyl cyanide 4-(trifluoromethoxy)phenylhydrazone (FCCP), and rotenone with antimycin A (both at 0.5 μM).

Glutamine uptake assay

Primary microglia were plated in 24-well cell culture plates 3 d before using. Cells were divided into two groups, the vehicle-treated and LPS-primed oAβ_{1-42} treated microglia. Each group of cells was treated as described above. Then, glutamine uptake assay was carried out. Mediums of each group was removed and replaced with cell culture medium containing 4 mM glutamine, and the mediums of each group was collected at 0, 2, 6 and 12 h (n=6 per time point). The mediums were analyzed by ThermoFisher Q-Exactive Orbitrap mass spectrometer equipped with ACQUITY UPLC BEH Amide column (100×2.1 mm, 1.7 μm; Waters) for obtaining the peak area of glutamine. The content values of glutamine were calculated by the peak area.

Mass spectrometry analysis of glutamine metabolism

The freshly isolated microglia from 8-month-old APP/PS1 mice or WT mice were washed with cold PBS and lysed with −80℃ methanol/water (50/50, v) on ice. Samples were centrifuged (14,000 × g, 4 ℃, 10 min) and an equal volume of methanol was added to the supernatant and centrifuged again. The supernatant was recovered and divided into two parts, one for the detection of amino acid metabolites and the other for the detection of TCA cycle intermediates.

For amino acids detection, a Waters XevoTQ-S triple quadrupole mass spectrometer equipped with ACQUITY UPLC BEH Amide column (100×2.1 mm, 1.7 μm; Waters) was useded for the separation of the metabolites. The gradient mobile phase was a mixture of acetonitrile/water (95/5, v) containing 0.1% ammonium acetate (A) and water containing 0.1% ammonium formate (B), and gradient elution was programmed as follows: 0–1 min, 5% B; 1–7 min, 5-50% B; 7–9 min, 50% B; 9–9.1 min, 50%-5% B; 9.1–12 min, 5%B; flow rate: 0.3 ml/min. The analytical column and autosampler temperatures were maintained at 45 °C and 4 °C, respectively. The injection volume was set at 5 μl.

For TCA cycle intermediates detection, 3-nitrophenylhydrazine (3-NPH) was used as a derivatizing reagent for the measurement of these organic acid. 100 μl samples were mixed with 50 μL aliquots of 3-NPH, 1-ethyl-3-(3-dimethylaminopropyl) carbodiimide (EDC), and pyridine. The 3-NPH, EDC, and pyridine solutions were prepared in methanol/water (75/25, v) to bring the final concentration to 50 mM, 30 mM and 1.5%, respectively. Once mixed, the solutions were reacted at 30℃ for 30 min, and then injected for analysis. A Waters Xevo TQ-S triple quadrupole mass spectrometer equipped with ACQUITY UPLC BEH C18 column (100×2.1 mm, 1.7 μm; Waters) was useded for the separation of the metabolites. The gradient mobile phase was a mixture of water containing 0.1% formic acid (A) and acetonitrile containing 0.1% formic acid (B), and gradient elution was programmed as follows: 0–2 min, 10–20% B; 2–9 min, 20-55% B; 9–10 min, 55–100% B; 10–11 min, 100% B; 11.1–13 min, 10%B; flow rate: 0.3 ml/min. The analytical column and autosampler temperatures were maintained at 45 °C and 4 °C, respectively. The injection volume was set at 5 μl.

Stable isotope tracing of glutamine

In the glutamine stable isotope tracing experiment, 4 mM $^{12}C_U$-glutamine in the DMEM medium (Glutamine free DMEM, Gibco) was replaced by 4 mM $^{13}C_U$-glutamine (Sigma-Aldrich). An untargeted stable isotope tracing strategy was applied to obtain the quantitative information of the relative incorporation of $^{13}C_U$-glutamine–derived metabolites. Waters ACQUITY UPLC I-Class liquid chromatography/Xevo G2-XS QTof mass spectrometer equipped with SeQuant ZIC-HILIC column (100×2.1 mm, 3.5 μm; Merck) was useded for the separation of the metabolites. The gradient mobile phase was a mixture of water containing 50 mM ammonium formate (A) and acetonitrile (B), and gradient elution was programmed as follows: 0–10 min, 90−50% B; 10–12 min, 50-90% B; 12–15 min, 90% B; flow rate: 0.4 ml/min. The analytical column and autosampler temperatures were maintained at 45 °C and 4 °C, respectively. The injection volume was set at 2 μl and the metabolites were monitored in full-scan mode (negative mode at a range of m/z 50-1200). The isotopologue spectral patterns identification was based on the monoisotopic molecular weight, MS/MS spectrum and the reference substance.

Mole percent enrichment measurement

The mole percent enrichment of each isotopologue was calculated as as follows:

$$\frac{\sum_{i=1}^{n} M_i \cdot i}{n}$$

n is the number of carbon atoms of the metabolite; M_i is the relative abundance of the i^{th} mass isotopomer.

Intracellular ROS production assays

A cell permeant fluorescent probe DCFH-DA (S0033S, Beyotime) was used for ROS detection. Primary microglia were plated in 24-well cell culture plates and washed with PBS twice. Cells were incubated with 10 μM DCFH-DA for 20 min at 37℃. Then, Cells were washed with serum free cell culture medium three times and cell images were observed using a fluorescence microscope (Nikon).

Small interference RNA

Primary microglia were treated with GLS1 small interfering RNA (GLS1 siRNA; SC-145431, Santa Cruz) for GLS1 knockdown, following the manufacturer's guidelines. siRNA or negative control siRNA (SC-44230, Santa Cruz) were diluted in lipofectamine RNAiMAX transfection reagent and Opti-MEM medium (Gibco) with the final concentration of 20 nM and incubated with primary microglia 24 h before LPS and oAβ_{1-42} treated.

Immunofluorescence

To detect the formation of LC3 puncta, primary microglia were seeded at a density of 1×10^6 cells/mL in coverslips coated with PLL in 6-well plates, washed 3 times with PBS and fixed with ice-cold 4% paraformaldehyde (PFA) for 35 min on ice. Then washed 3 times with PBS and permeabilized using 0.5% triton X-100 (Sigma-Aldrich) for 15 min. Washed 3 times with PBS and blocked in 5% BSA (Sigma-Aldrich) for 1.5 h at room temperature (RT). The coverslips were then stained with rabbit polyclonal anti-LC3 (1:100; 18725-1-AP, Proteintech) overnight at 4℃. Washed coverslips 3 times with PBS and incubated with goat anti-rabbit Alexa fluor 488 (1:500; SA00013-2, Proteintech) for 2 h at room temperature and the cell nuclei were stained with DAPI for 5 min at room temperature.

To determine the co-localization of TOM20 with LAMP1 or co-localization of ASC with NLRP3 using immunofluorescence, primary microglia were seeded at a density of 1×10^6 cells/mL in coverslips coated with PLL in 6-well plates. After fixed with 4% PFA, permeabilized using 0.5% triton X-100 and blocked in 5% BSA, the coverslips were then stained with mouse monoclonal anti-TOM20 (1:200; 66777-1-Ig, Proteintech) and rabbit polyclonal anti-LAMP1 (1:100; bs-1970R, Bioss) or goat polyclonal anti-ASC (1:50; ab175449, Abcam) and rabbit polyclonal anti-NLRP3 (1:500; 19771-1-AP, Proteintech) overnight at 4℃. Washed coverslips 3 times with PBS and incubated with goat anti-mouse Alexa 488 (1:500; SA00013-1, Proteintech) and goat anti-rabbit Alexa 594 (1:500; SA00013-4, Proteintech) or donkey anti-goat Alexa 488 (1:500; ab150129, Abcam) and goat anti-rabbit Alexa 594 (1:500; SA00013-4, Proteintech) for 2 h at room temperature. Cell nuclei were stained with DAPI for 5 min at room temperature. Cell images were acquired on a Leica TCS SP8 confocal microscope (Leica).

Mitochondrial membrane potential analysis

Mitochondrial membrane potential of primary microglia was measured using a JC-1 probe (C2006, Beyotime) following the manufacturer's guidelines. Briefly, cells were stained with JC-1 (1×) for 20 min at 37℃, and then washing twice with free cell culture medium and cell images were acquired on a Leica TCS SP8 confocal microscope (Leica).

Mitochondria-lysosome co-localization analysis

After corresponding treatment, primary microglia were co-stained with 100 nM LysoTracker Green (G1722, Servicebio) and 500 nM MitoTracker Red (G1723, Servicebio) for 1 h under normal cell culture conditions. Replace the culture medium with a new DMEM and observe with a Leica TCS SP8 confocal microscope (Leica).

Statistical analysis

Statistical analysis was performed using GraphPad Prism v8 software for unpaired Student's t-test or One way ANOVA. All data were presented as means±standard error of the mean (SEM) for at least in triplicate.

Results

NLRP3 inflammasome activation is accompanied by metabolomic changes of microglia in the pathogenesis of AD

To better understand the mechanism responsible for initiation of inflammatory response in microglia in AD, an APP/PS1 transgenic mouse model of AD was employed. Consistent with previous studies, the 8-month-old female APP/PS1 mice exhibited greater Aβ deposition (Supplementary Fig. S1A), activated microglia (Supplementary Fig. S1B), and total soluble Aβ and Aβ_{1-42} (Supplementary Fig. S1C) in hippocampal tissue compared to those in their wild-type (WT) littermates. Aβ deposition in AD is accepted as an effect of stimulating microglial inflammatory response in AD, and can induce the activation of NLRP3 inflammasomes, which subsequently cleave pro-IL-1β, pro-IL-18, and gasdermin D into their active forms [4, 30]. In line with previous reports, we observed an increase in the content of IL-1β and IL-18 (Supplementary Fig. S1D), as well as the levels of NLRP3, pro-IL-1β, mature IL-1β (p17), and mature caspase-1 (p20)

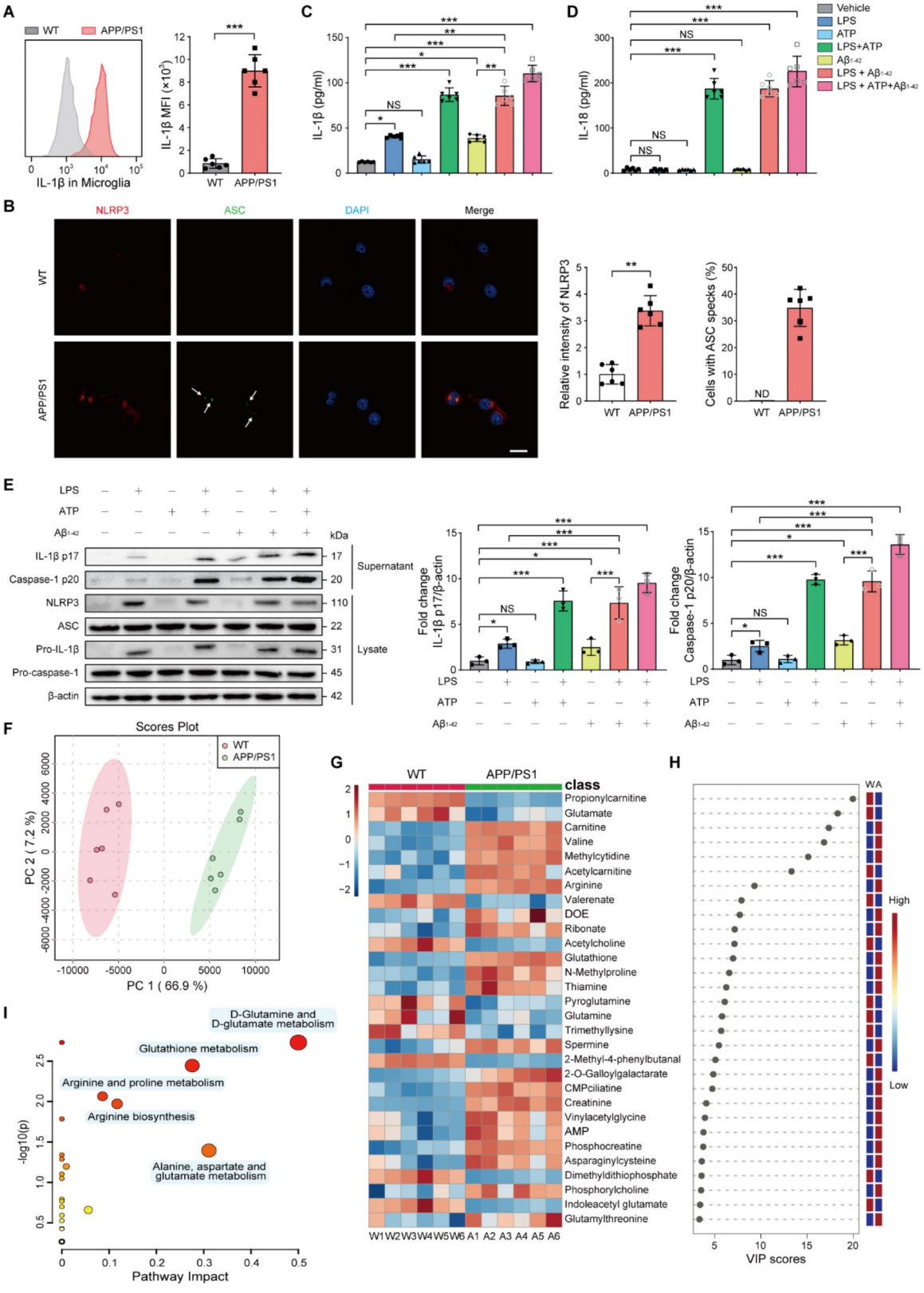

Fig. 1 (See legend on next page.)

(See figure on previous page.)

Fig. 1 NLRP3 inflammasome activation is accompanied by metabolomic changes of microglia in the pathogenesis of AD. (**A**) Flow cytometry to detect the protein expression of IL-1β as mean fluorescence intensity (MFI) in microglia from 8-month-old female APP/PS1 mice (red lines and bars) or WT mice (gray lines and bars) ($n=6$). (**B**) Representative immunofluorescence staining of NLRP3 (red), ASC (green), and DAPI (blue) in microglia from 8-month-old female APP/PS1 mice or WT mice. White arrows indicate ASC specks. ND, not detected. Scale bar: 10 μm ($n=6$). (C and D) ELISA assays quantifying IL-1β (**C**) and IL-18 (**D**) secretion in culture supernatants of primary microglia pre-treated with LPS (100 ng/ml, 6 h) before ATP (5 mM, 4 h) or $oA\beta_{1-42}$ (5 μM, 12 h) treatment ($n=6$). (**E**) Western blot analysis of cell supernatants or lysates to detect mature IL-1β and caspase-1, NLRP3, ASC, pro-IL-1β, pro-caspase-1 and β-actin in primary microglia pre-treated with LPS (100 ng/ml, 6 h) before ATP (5 mM, 4 h) or $oA\beta_{1-42}$ (5 μM, 12 h) treatment ($n=3$). (**F**) Principal component analysis of metabolomics profiles for the isolated microglia from 8-month-old female APP/PS1 mice or WT mice ($n=6$). (**G**) Heatmap of the isolated microglia between the 8-month-old female WT and APP/PS1 mice subjected to metabolomic profiling. Shown are only the 30 most significantly different metabolites ranked by the variable importance in projection (VIP) scores ($n=6$). W1–W6 represents WT mice and A1–A6 represents APP/PS1 mice. (**H**) VIP plot identified by partial least squares discriminant analysis (PLS-DA) displaying the top 30 most important metabolite features in the isolated microglia of the 8-month-old female WT or APP/PS1 mice. The bar on the right indicates whether each metabolite is enhanced (red) or depleted (purple) in each group ($n=6$). Metabolic Pathway Enrichment Analysis using putatively identified metabolites of the isolated microglia between the 8-month-old female WT and APP/PS1 mice. Pathway impact is measured by the percentage of metabolites in a given pathway and their relative importance in that pathway. n represents the number of biological replicates. Data are presented as the mean ± SEM. Statistical significance was determined by unpaired Student's t test (**A** and **B**) or one-way ANOVA (C-E). $^{*}p<0.05$; $^{**}p<0.01$; $^{***}p<0.001$; NS, not significant

in the hippocampus of APP/PS1 mice compared with that in WT mice (Supplementary Fig. S1E). To investigate whether NLRP3 inflammasome was activated in microglia under AD pathology, we compared the IL-1β level on freshly isolated microglia ($CD11b^+$ microglia) from 8-month-old female APP/PS1 mice or WT mice. As expected, microglia of APP/PS1 mice showed higher levels of IL-1β than WT mice (Fig. 1A). Additionally, we conducted immunofluorescence co-localization experiments for NLRP3 and ASC pecks in $CD11b^+$ microglia, and the results revealed a significant increase in NLRP3 and ASC pecks in the microglia of APP/PS1 mice, indicating activation of the NLRP3 inflammasome (Fig. 1B).

To confirm that Aβ indeed triggered NLRP3 inflammasome activation in microglia, we treated LPS-primed primary microglia with oligomeric $A\beta_{1-42}$ ($oA\beta_{1-42}$, Supplementary Fig. S2A) or the specific NLRP3 inflammasome activator ATP, then quantified IL-1β and IL-18 secretion. Generally, NLRP3 inflammasomes require a priming signal from the NF-κB pathway, which induces the expression of NLRP3, pro-IL-1β, and pro-IL-18 via Toll-like receptors [31]. In the activation stage, NLRP3 senses corresponding associated molecular patterns, such as ATP, nigericin, crystalline substances and Aβ, then assembles and activates the NLRP3 inflammasome [32–34]. The results showed that in microglia exposed to LPS, $oA\beta_{1-42}$ induced an increase in IL-1β (Fig. 1C) and IL-18 (Fig. 1D) secretion compared to that in cells without LPS pre-incubation. The effect of $oA\beta_{1-42}$ on NLRP3 inflammasome activation was confirmed by Western blot (WB) analysis, based on results showing that cleaved IL-1β (p17) and caspase-1 (p20) levels were increased in culture supernatants of LPS-primed microglia treated with $oA\beta_{1-42}$, while NLRP3, ASC, pro-IL-1β and pro-caspase-1 expression were unchanged (Fig. 1E and Supplementary Fig. S2B). These results suggest that $oA\beta_{1-42}$ affects the activation signal for NLRP3 inflammasomes, but not the priming signal. $oA\beta_{1-42}$ also promoted the cleavage of gasdermin D to its active N-terminal fragment (Supplementary Fig. S2C) in LPS pre-incubation microglia. However, it does not increase the release of LDH (Supplementary Fig. S2D), which is used as a measure of pyroptosis, indicating that $oA\beta_{1-42}$ promotes NLRP3 inflammasome activation without inducing cell death in LPS pre-incubation microglia. Therefore, LPS-primed $oA\beta_{1-42}$-treated microglia (LoAMs) were used to mimic the activation of NLRP3 inflammasome in microglia under AD pathological conditions.

To investigate how NLRP3 inflammasome activity contributes to AD pathology, untargeted mass spectrometry-based metabolomics was conducted to identify the polar metabolites of $CD11b^+$ microglia or cultured primary microglia. 3274 metabolites of $CD11b^+$ microglia were measured and then analyzed using the MetaboAnalyst software. Principal component analysis (PCA) showed a good separation between APP/PS1 mice and WT mice (Fig. 1F), indicated that AD had caused the disorder of metabolites in microglia. Statistical analysis revealed 313 significantly different metabolites between the $CD11b^+$ microglia of APP/PS1 and WT mice (variable importance in the projection (VIP) > 1, Supplementary Table S1). Subsequent heatmap analysis of the 30 most significantly different metabolites defined specific metabolic signatures for the APP/PS1 and WT mice (Fig. 1G, H). Metabolic pathway enrichment analysis showed marked changes in several metabolic pathways in the $CD11b^+$ microglia under AD pathology, especially "glutamine and glutamate metabolism", "glutathione metabolism", "alanine and proline metabolism", "arginine biosynthesis", and "alanine, aspartate and glutamate metabolism" (Fig. 1I). Concurrently, untargeted metabolomics was used to broadly identify differences in intracellular metabolites related to NLRP3 inflammasome activation in vehicle-, LPS-, $oA\beta_{1-42}$- treated primary microglia and LoAMs. The PCA results showed a clear changed of microglia metabolism after LPS and $oA\beta_{1-42}$ treatment (Supplementary Fig. S2E). Consistent with metabolomics analysis of $CD11b^+$ microglia, glutamine and glutamate were

both significantly different in LoAMs, but not in the LPS- or oAβ_{1-42}- treated microglia (Supplementary Fig. S2F). In particular, glutamine-related metabolic pathways were markedly disrupted in LoAMs (Supplementary Fig. S2G). Taken together, these results indicated that NLRP3 inflammasomes were activated in microglia during AD development and this process may be accompanied by metabolomic changes dominated by glutamine metabolism.

Glutamine is rapidly metabolized upon NLRP3 inflammasome activation in microglia

Based on these above findings, we next investigated the relationship between NLRP3 inflammasome activation and changes in microglial glutamine metabolism. To this end, we first compared differences in metabolic requirements between vehicle-treated microglia and LoAMs through measuring the oxygen consumption rate (OCR), as an indicator of oxidative phosphorylation (OXPHOS) using a Seahorse XF analyzer. The OCR was higher in LoAMs compared with vehicle-treated microglia, implying that the sequential treatment of LPS and oAβ_{1-42} promotes the metabolism of microglia (Fig. 2A). In addition, a glutamine uptake assay showed that the extracellular glutamine consumption rate was significantly higher during oAβ_{1-42} stimulation with LPS priming (Fig. 2B). These results suggested that glutamine utilization by microglia was elevated during NLRP3 inflammasome activation, triggered by LPS and oAβ_{1-42} stimulation. We therefore next explored the possible functions of glutamine in microglia during NLRP3 inflammasome activation. Since glutamine has multiple metabolic uses, but in rapidly proliferating cells it mainly serves in anaplerotic replenishment of TCA cycle intermediates [27, 28] (Fig. 2C), we hypothesized that glutamine anaplerosis is essential for NLRP3 inflammasome activation.

To test this possibility, targeted metabolomics was initially used to identify common differences in glutamine-derived intracellular metabolite levels between the CD11b$^+$ microglia of APP/PS1 and WT mice. Liquid chromatography-mass spectrometry (LC-MS) showed that levels of glutamine, glutamate, α-ketoglutaric acid, succinate, citrate and aspartate were all decreased in CD11b$^+$ microglia of APP/PS1 mice (Fig. 2D). Furthermore, this analysis indicated that amino acids, such as alanine, proline, arginine, citrulline and ornithine were all increased in these CD11b$^+$ microglia relative to their levels of WT mice (Fig. 2D). Notably, each of these metabolites were derived from glutamine deamination and subsequent metabolic steps (Fig. 2C), which suggested that the increased use of glutamine by microglia after NLRP3 inflammasome activation may be related to an accelerated flux of glutamine to derivative amino acids.

Reduced glutamine metabolism regulates NLRP3 inflammasome activation of microglia in the pathogenesis of AD

Given that GLS1 is primarily responsible for catalyzing glutamine metabolism, we inhibited GLS1 to test whether the increase in glutamine utilization was related to the observed increase in NLRP3 inflammasome activation. For this purpose, we quantified the release of active IL-1β (p17) and caspase-1 (p20) in culture supernatants of LPS-primed oAβ_{1-42}-treated microglia with NLRP3 inflammasome activation after inhibition of GLS1 with the small molecule inhibitor BPTES [35] (Supplementary Fig. S3A) or by GLS1 knockdown via GLS1 siRNA (Supplementary Fig. S3B) in vitro. We found that active IL-1β and caspase-1 release was significantly limited under GLS1 inhibition (Fig. 3A, B), while pro-IL-1β and pro-caspase-1 expression were unchanged (Supplementary Fig. S3C, S3D), suggesting that down-regulation of glutamine metabolism via GLS1 inhibition can block NLRP3 inflammasome activity in microglia. To verify the inhibitory effect of GLS1 on the NLRP3 inflammasome, we assessed its impact on ASC speck formation in microglia. Consistent with its effects on IL-1β and caspase-1, BPTES or GLS1 siRNA suppressed oAβ_{1-42}-induced ASC speck formation (Fig. 3C). Besides, in order to investigate whether this effect is specific to NLRP3 inflammasome, we analyzed the release of IL-1β in microglia, which were pre-treatment with BPTES or GLS1 siRNA before treatment with LPS and ATP, an NLRP3 inflammasome activator, or poly(dA: dT), an AIM2 inflammasome activator, or flagellin, an NLRC4 inflammasome activator, or muramyl dipeptide (MDP), an NLRP1 inflammasome activator. Our results showed that both BPTES and GLS1 siRNA suppressed IL-1β release in response to treatment with NLRP3 inflammasome activator (Supplementary Fig. S3E, S3F). However, BPTES or GLS1 siRNA had no effect on IL-1β cleavage in response to treatment with poly(dA: dT), flagellin or MDP (Supplementary Fig. S3E, S3F), which indicated that GLS1 inhibition has a specific targeting of NLRP3 inflammasome.

We then treated APP/PS1 mice with Telaglenastat (CB-839) in vivo, a chemical inhibitor that attenuates GLS1 expression and therefore its downstream glutamine metabolism [36]. After one week of continuous injection, the effects of CB-839 on microglia and NLRP3 inflammasome activation in the brain of APP/PS1 mice were investigated. The immunohistochemical staining results showed that CB-839 treatment can significantly inhibit the activation of microglia (Fig. 3D) and Aβ deposition (Supplementary Fig. S3E). At the same time, flow cytometry analysis of CD11b$^+$ microglia of APP/PS1 mice revealed a significant decrease in mature IL-1β (Fig. 3E) and caspase-1 (Fig. 3F) level after treatment with CB-839, indicating that CB-839 can inhibit NLRP3 inflammasome

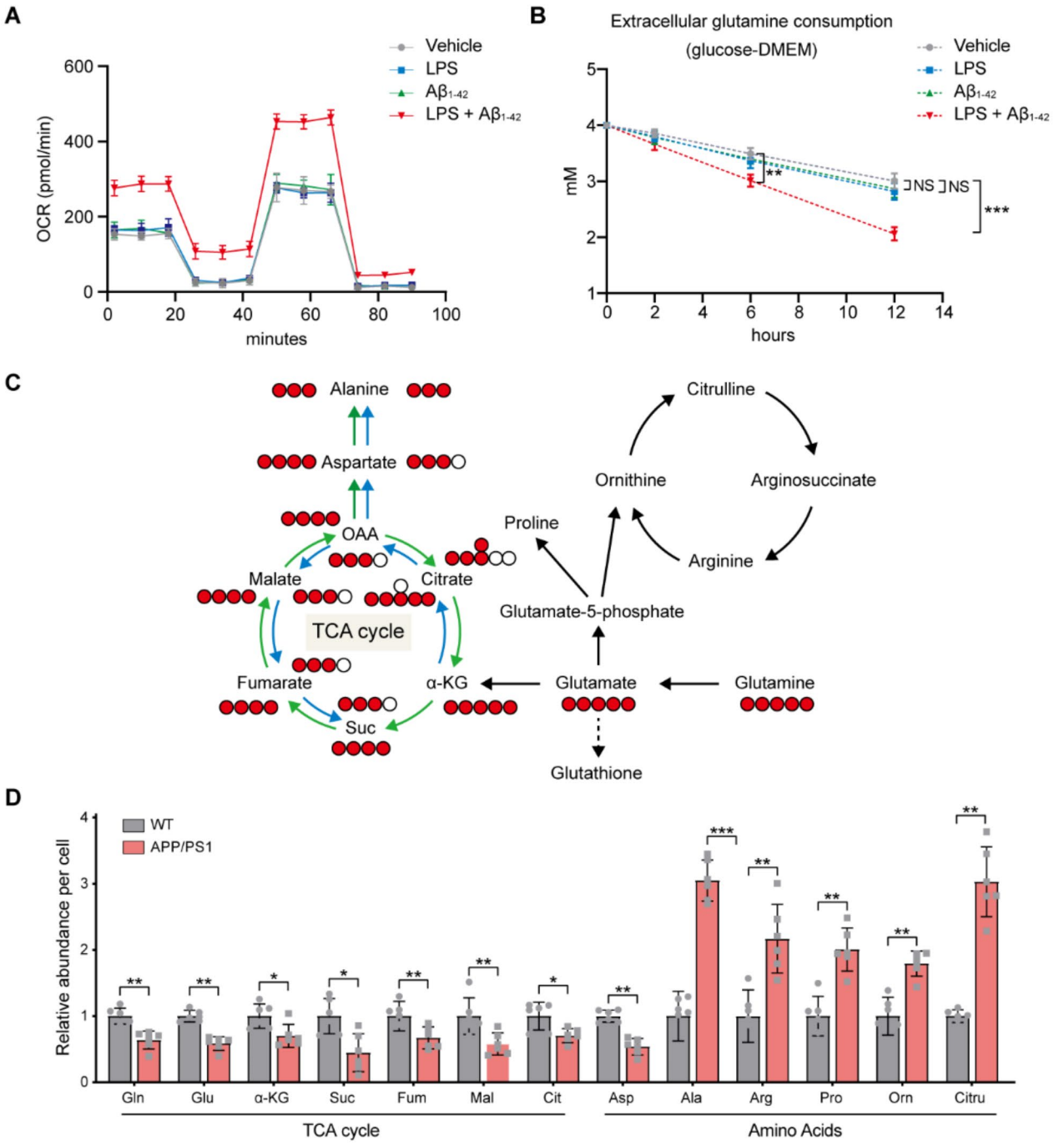

Fig. 2 Glutamine is rapidly metabolized upon NLRP3 inflammasome activation in microglia. (**A**) Seahorse analysis of oxygen consumption rate (OCR) in vehicle-, LPS-, oAβ_{1-42}- treated microglia and LoAMs ($n=3$). (**B**) Extracellular levels of glutamine in vehicle-, LPS-, oAβ_{1-42}- treated microglia and LoAMs after culture for 2, 6, and 12 h in glucose-DMEM ($n=6$). (**C**) Metabolic network connecting amino acids of interest through dominant glutamine-glutamate pathways, and schematic representation of oxidative (outer ring in green) and reductive (inner ring in blue) glutamine anaplerotic flux. Open circles depict ^{12}C and filled red circles depict ^{13}C atoms derived from $^{13}C_U$-glutamine. (**D**) Relative intracellular metabolite abundance measured by mass spectrometry in CD11b$^+$ microglia of APP/PS1 mice normalized by cell number and CD11b$^+$ microglia of WT mice ($n=6$). n represents the number of biological replicates. Data are presented as the mean ± SEM. Statistical significance was determined by one-way ANOVA. *$p<0.05$; **$p<0.01$; ***$p<0.001$; NS, not significant. Gln, glutamine; Glu, glutamate; α-KG, α-ketoglutaric acid; Suc, succinate; Fum, fumarate; Mal, malate; Cit, citrate; OAA, oxaloacetate; Asp, aspartate; Ala, alanine; Arg, arginine; Pro, proline; Orn, ornithine; Citru, citrulline

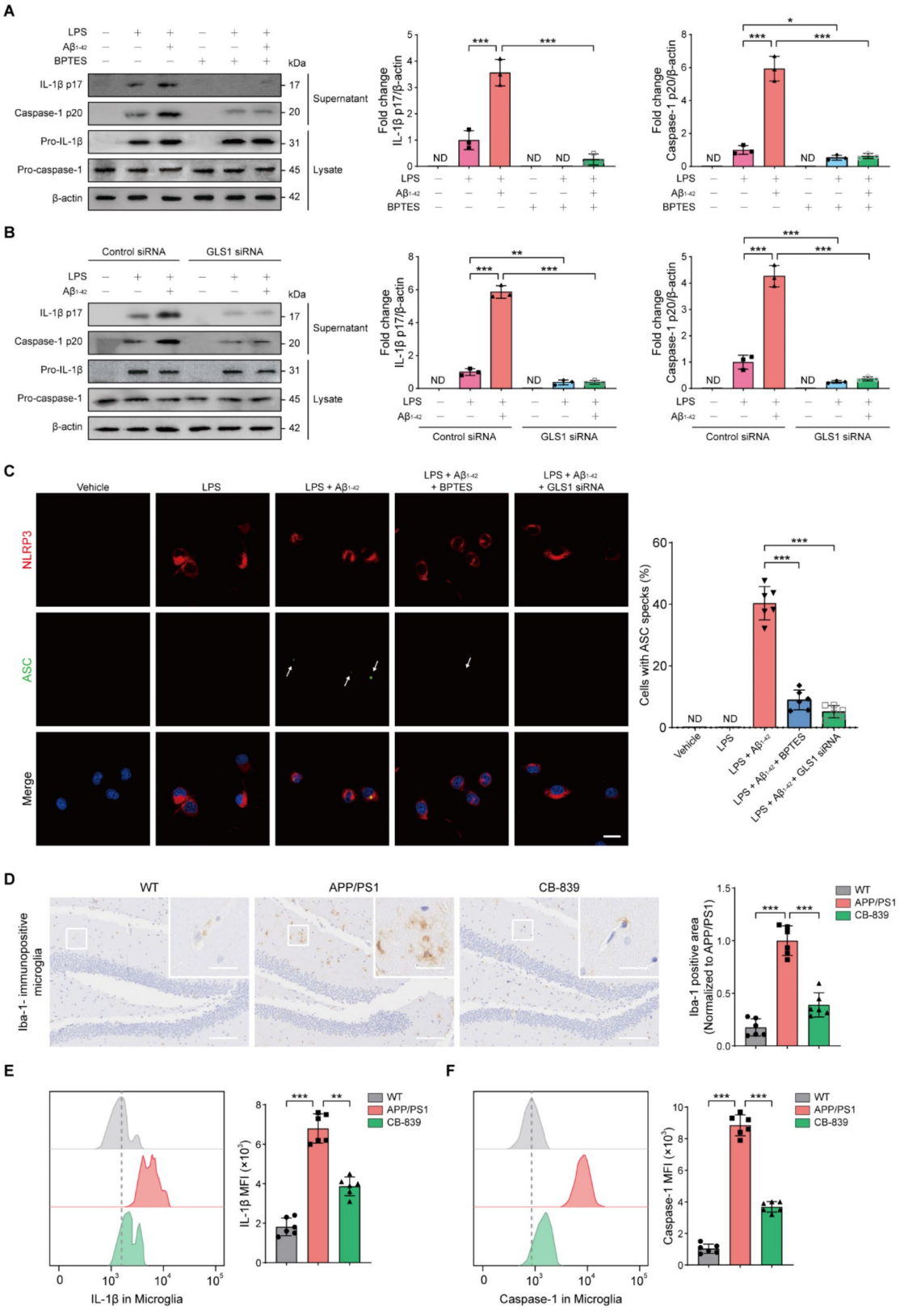

Fig. 3 (See legend on next page.)

(See figure on previous page.)

Fig. 3 Reduced glutamine metabolism regulates NLRP3 inflammasome activation of microglia in the pathogenesis of AD. (A and B) WB analysis of pro- and mature caspase-1 and IL-1β in lysates and supernatants of LoAMs under GLS1 suppression by BPTES (**A**) or siRNA (**B**) ($n=3$). ND, not detected. (**C**) Representative immunofluorescence staining of NLRP3 (red), ASC (green), and DAPI (blue) in primary microglia before or after LPS (100 ng/mL, 6 h) priming followed by oAβ_{1-42} (5 μM, 12 h) in the presence or absence of BPTES or GLS1 siRNA. White arrows indicate ASC specks. ND, not detected. Scale bar: 10 μm ($n=6$). (**D**) Iba1-immunopositive microglia and quantitative analysis of microglia in the hippocampal regions of 8-month-old female WT and APP/PS1 mice ($n=6$). Scale bar: 200 μm. The insets show the magnified Iba1-immunopositive microglia. Scale bar: 50 μm. (E and F) Flow cytometry to detect the protein expression of IL-1β (**E**) and caspase-1 (**F**) as mean fluorescence intensity (MFI) in microglia from 8-month-old WT mice (gray lines and bars) or APP/PS1 mice in the presence (green lines and bars) or absence (red lines and bars) of CB-839 ($n=6$). n represents the number of biological replicates. Data are presented as the mean ± SEM. Statistical significance was determined by one-way ANOVA. *$p<0.05$; **$p<0.01$; ***$p<0.001$

activation. Collectively, these findings indicate that inhibiting glutamine metabolism may consequently decrease NLRP3 inflammasome and relieve neuroinflammation of AD.

Reduced glutamine metabolism hinders glutamine anaplerotic flux and amino acid synthesis in LPS-primed oAβ_{1-42}-treated primary microglia

To better understand the metabolic fate of glutamine in microglia, we used stable isotope-labeled glutamine to trace the relative metabolic flux of glutamine after LPS and oAβ_{1-42}-induced NLRP3 inflammasome activation. Briefly, the vehicle-treated microglia and LoAMs were precultured in glucose-DMEM, then incubated with a glutamine tracer uniformly labeled with ^{13}C ($^{13}C_U$-glutamine) for 6 h. The distribution of the tracer in TCA cycle metabolites and related intermediates was determined by measuring the mass isotope-labeling pattern (Fig. 4A). In this tracer experiment, $^{13}C_U$-glutamine subjected to oxidative TCA cycle metabolism (Fig. 2C) should generate (M+4) forms of succinate, malate, aspartate and citrate, due to the incorporation of four ^{13}C atoms in each of these species. By contrast, reductive carboxylation should yield (M+5) forms of citrate (i.e., through incorporation of five ^{13}C atoms) and (M+3) forms of succinate, malate and aspartate (i.e., through incorporation of three ^{13}C atoms; see schematic in Fig. 2C). Thus, the relative contributions of oxidative metabolism versus reductive carboxylation arising from glutamine anaplerosis can be reliably quantified by determining the isotopologue distribution and enrichment with ^{13}C in TCA cycle intermediates.

The results indicated that glutamate (M+5) (Fig. 4B and Supplementary Fig. S4A), α-ketoglutaric acid (M+5) (Fig. 4C and Supplementary Fig. S4B), succinate (M+4 and M+3) (Fig. 4D and Supplementary Fig. S4C), malate (M+4 and M+3) (Fig. 4E and Supplementary Fig. S4D), and aspartate (M+4 and M+3) (Fig. 4F and Supplementary Fig. S4E) derived from $^{13}C_U$-glutamine were all significantly increased in LPS-primed oAβ_{1-42}-treated microglia following NLRP3 inflammasome activation, compared with their levels in vehicle-treated microglia. By contrast, the total abundance of each metabolite, including the total labeled and unlabeled isotopologues, decreased after LPS and oAβ_{1-42} stimulation (Supplementary Fig. S4F), which was consistent with the results of targeted metabolomics of the CD11b$^+$ microglia from 8-month-old APP/PS1 mice or WT mice (Fig. 2D). In addition, the M+4 isotopologues of succinate, malate, and aspartate were markedly more abundant than the corresponding M+3 isotopologues, which indicated that oxidative metabolism was the predominant mode of glutamine anaplerosis. Overall, the decreased total abundances of glutamate, α-ketoglutaric acid, succinate, malate, and aspartate, together with the increased isotopologue distribution with ^{13}C, consistently indicated a faster glutamine flux through the glutamine anaplerosis in microglia following LPS and oAβ_{1-42} stimulation as compared with the control group.

Due to the complexity of metabolic pathways responsible for the fate of glutamine-derived amino acids (including proline, arginine, citrulline, and ornithine), accurate determination of the role of glutamine in their synthesis was difficult through single isotope labeling. Therefore, the contribution of glutamine carbon to amino acid synthesis was calculated as the proportion of each amino acid isotopologue to their respective total abundance. We found that glutamine carbon integration into amino acids was increased in LPS-primed oAβ_{1-42}-treated microglia compared with that in vehicle-treated microglia (Fig. 4G and Supplementary Fig. S4G). Collectively, these results indicated that in microglia with activated NLRP3 inflammasomes, oxidative metabolism and reductive carboxylation were both increased through glutamine anaplerosis, as was synthesis of glutamine-derived amino acids.

Next, we investigated the effects of GLS1 inhibition on glutamine anaplerotic flux. In line with our above results, tracing studies revealed that glutamate (M+5) (Fig. 4B), α-ketoglutaric acid (M+5) (Fig. 4C), succinate (M+4 and M+3) (Fig. 4D), malate (M+4 and M+3) (Fig. 4E), and aspartate (M+4 and M+3) (Fig. 4F) isotopologues were all significantly decreased under GLS1 suppression by BPTES or siRNA compared with their levels under NLRP3 inflammasome activation stimulated by LPS and oAβ_{1-42}. In addition, glutamine incorporation into proline, arginine, citrulline, and ornithine was also prevented by GLS1 suppression (Fig. 4G). These results indicated that deficiency for GLS1 in microglia can weaken the oxidative metabolism and reductive carboxylation required

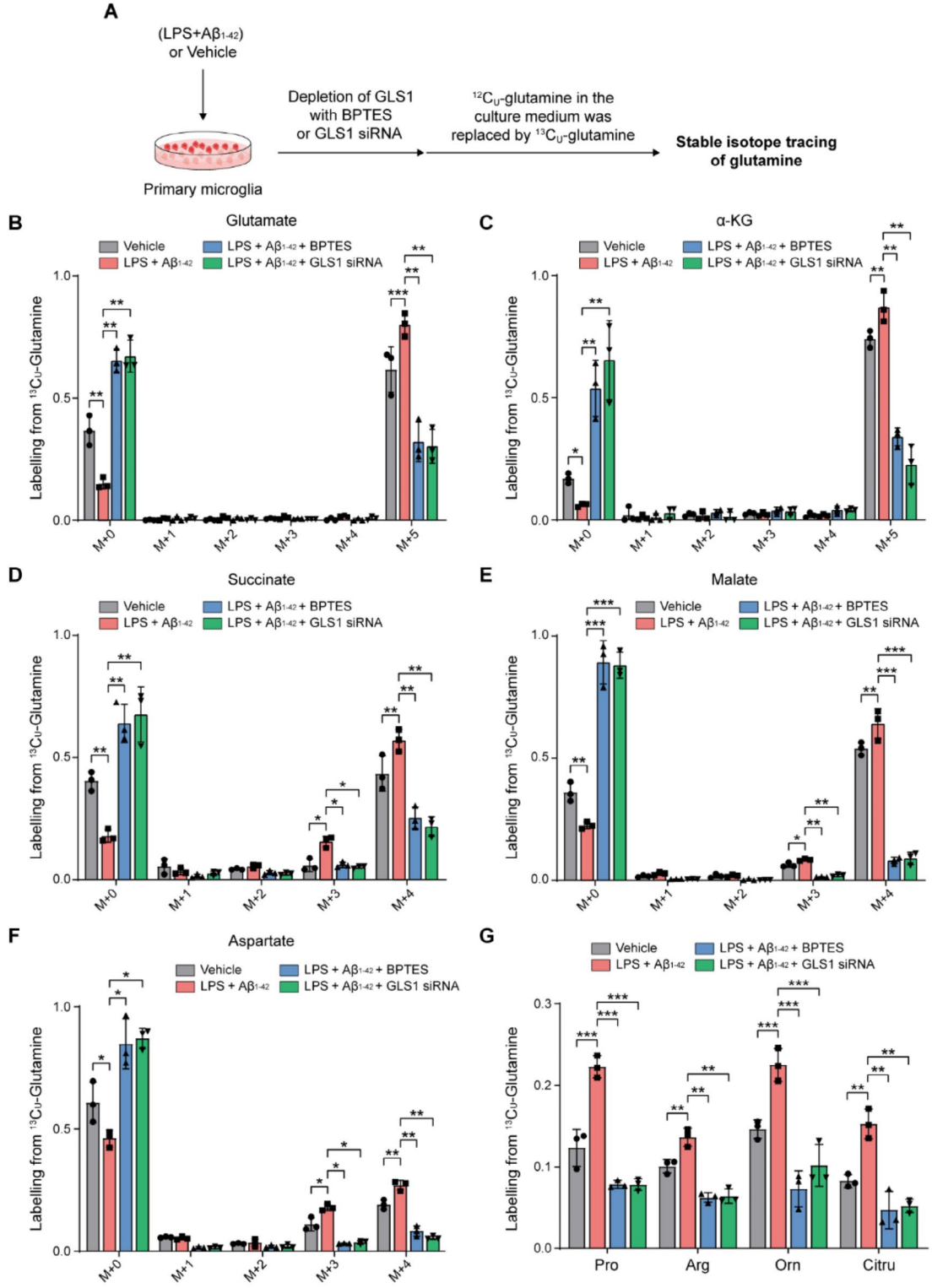

Fig. 4 Reduced glutamine metabolism hinders glutamine anaplerotic flux and amino acid synthesis in LPS-primed oAβ_{1-42}-treated primary microglia. (**A**) Experimental scheme for stable isotope tracing of glutamine. (B-F) Effect of BPTES and GLS1 siRNA on fractional contribution of $^{13}C_U$-glutamine to glutamate (**B**), α-KG (**C**), succinate (**D**), malate (**E**) and aspartate (**F**) ($n=3$). (**G**) Effect GLS1 suppression by BPTES or GLS1-targeted siRNA on fractional contribution of $^{13}C_U$-glutamine to glutamine-derived amino acids ($n=3$). n represents the number of biological replicates. Data are presented as the mean ± SEM. Statistical significance was determined by one-way ANOVA. *$p<0.05$; **$p<0.01$; ***$p<0.001$

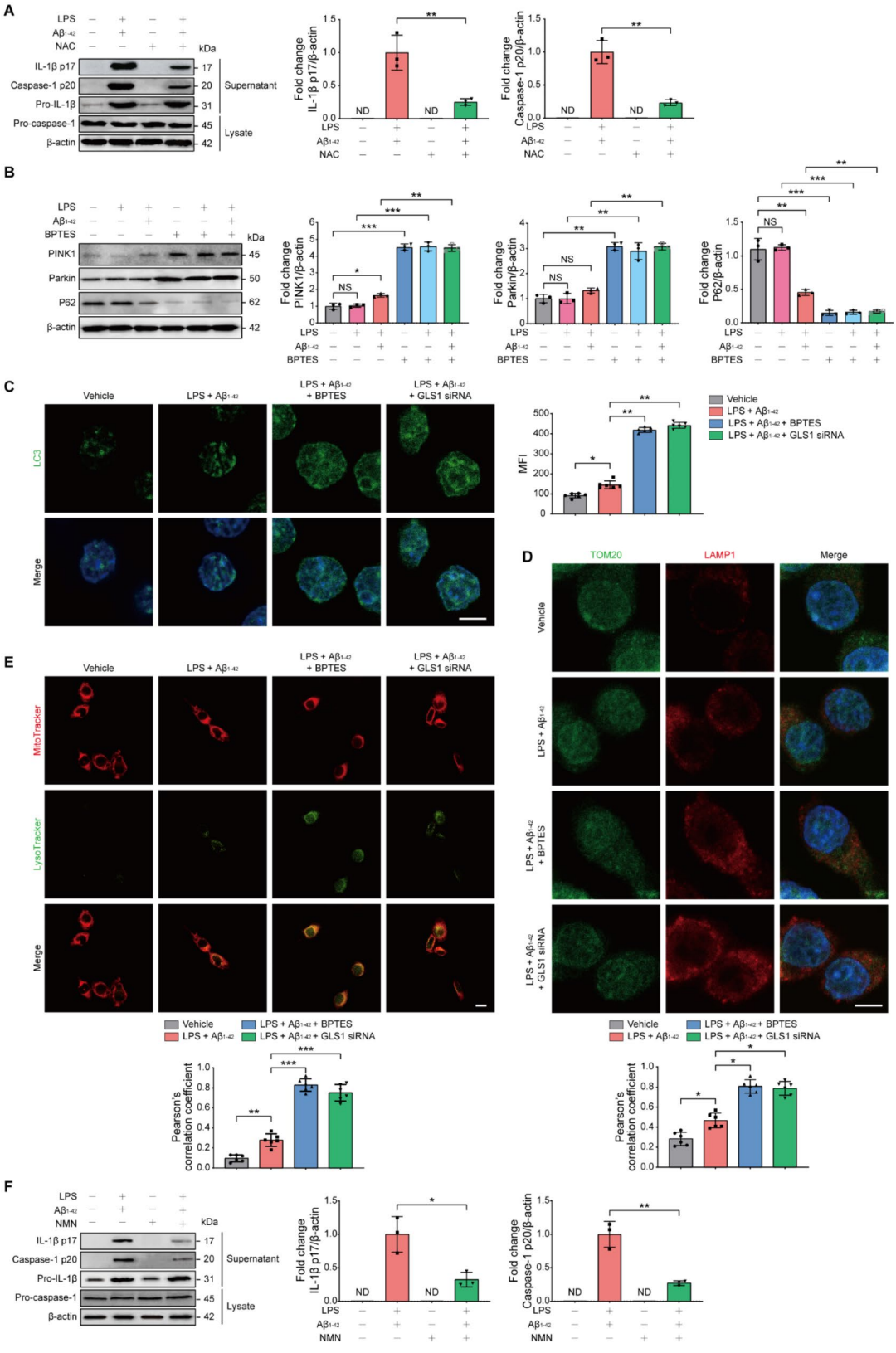

Fig. 5 (See legend on next page.)

(See figure on previous page.)

Fig. 5 Reduced glutamine metabolism enhances microglial mitophagy and inhibits NLRP3 inflammasome activation. (**A**) Western blots of pro- and mature IL-1β and caspase-1 in lysates and supernatants of LoAMs in the presence or absence of the anti-oxidant and free radical scavenger NAC ($n=3$). ND, not detected. (**B**) Western blots and densitometry quantification of the mitophagy protein PINK1, parkin, and p62 in LoAMs in the presence or absence of BPTES ($n=3$). (**C**) Autophagosome formation indicated by puncta and quantitated by confocal microscopy in LoAMs in the presence or absence of BPTES or GLS1 siRNA. Scale bar: 10 μm ($n=6$). (**D**) Confocal microscopy detection and quantitation of co-localization of the mitochondrial protein TOM20 (green), lysosomal protein LAMP1 (red), and DAPI (blue) in LoAMs in the presence or absence of BPTES or GLS1 siRNA. Scale bar: 10 μm ($n=6$). (**E**) Confocal microscopy detection and quantitation of co-staining of MitoTracker ang LysoTracker in LoAMs in the presence or absence of BPTES or GLS1 siRNA. Scale bar: 10 μm ($n=6$). (**F**) WB analysis of pro- and mature IL-1β and caspase-1 in lysates and supernatants of LoAMs in the presence or absence of mitophagy stimulator NMN ($n=3$). n represents the number of biological replicates. Data are presented as the mean ± SEM. Statistical significance was determined by one-way ANOVA. *$p<0.05$; **$p<0.01$; ***$p<0.001$

for glutamine anaplerosis, and inhibits biosynthesis of glutamine-derived amino acids.

Reduced glutamine metabolism enhances microglial mitophagy and inhibits NLRP3 inflammasome activation

We next investigated the regulatory mechanism through which glutamine metabolism mediates NLRP3 inflammasome activation in the pathogenesis of AD. Higher ROS accumulation was detectable in LoAMs compared with that in vehicle-treated microglia, while GLS1 knockdown by BPTES or GLS1 siRNA treatment resulted in significantly reduced ROS production compared with untreated control cells (Supplementary Fig. S5A). It is noteworthy that ROS are presumed to directly trigger NLRP3 inflammasome activation [32]. Pretreatment of microglia with the ROS scavenger NAC resulted in significant inhibition of the release of mature IL-1β and caspase-1 (Fig. 5A and Supplementary Fig. S5B). These data implied that glutamine metabolism may affect NLRP3 inflammasome activation through modulation of ROS production.

It is well-established that mitochondrial dysfunction can result in elevated ROS production [37], so we therefore evaluated the effects of glutamine metabolism on mitochondrial function during activation of NLRP3 inflammasomes. Compared with vehicle-treated microglia, LoAMs exhibited reduced mitochondrial membrane potential, as assessed by JC-1 assays (Supplementary Fig. S5C), and was accompanied by increased levels of the mitochondrial matrix protein, m-aconitase (Supplementary Fig. S5D, S5E), suggesting that dysfunctional mitochondria might accumulate during NLRP3 inflammasome activation stimulated by LPS and oAβ_{1-42}. It noteworthy that these effects were markedly inhibited under GLS1 silencing by BPTES (Supplementary Fig. S5D) or GLS1 siRNA (Supplementary Fig. S5E). These results collectively showed that inhibition of glutamine metabolism in microglia with activated NLRP3 inflammasomes might alleviate mitochondrial dysfunction, which may potentially serve as a determining factor in the regulation of NLRP3 inflammasome activation.

Since mitophagy is essential for clearance of damaged mitochondria and maintenance of cellular homeostasis [38], we thus hypothesized that suppression of glutamine metabolism could inhibit activation of NLRP3 inflammasomes by promoting mitophagy and consequently reducing intracellular ROS production. WB assays showed that expression of the mitophagy-related protein PINK1 and parkin was increased and the expression of p62 was decreased in LoAMs, compared with that in vehicle-treated microglia, while GLS1 inhibition by BPTES (Fig. 5B) or GLS1 siRNA (Supplementary Fig. S5F) led to a further increase in PINK1 and parkin levels and a further decrease in p62 levels. Immunofluorescence microscopy revealed increased expression of the autophagosomal microtubule-associated protein 1 A-1B-light chain 3 (LC3) (Fig. 5C) and increased co-localization of outer mitochondrial membrane protein TOM20 with lysosomal-associated membrane protein 1 (LAMP1) in BPTES- or GLS1 siRNA-treated microglia compared with LoAMs, indicating that damaged mitochondria were efficiently delivered to lysosomes (Fig. 5D). To further confirm this, we performed immunofluorescence staining of MitoTracker and LysoTracker. BPTES- or GLS1 siRNA-treated microglia displayed a significantly increased MitoTracker and LysoTracker merge staining (yellow) compared with LoAMs (Fig. 5E). These results indicated that inhibiting glutamine metabolism in microglia with activated NLRP3 inflammasomes could enhance mitophagy-mediated clearance of damaged mitochondria.

To test this possibility, LoAMs were exposed to NMN, a stimulator of mitophagy, and NLRP3 inflammasome activity was determined by quantification of IL-1β and caspase-1. The results indicated that levels of both proteins were decreased under stimulation of mitophagy compared with unstimulated cells (Fig. 5F and Supplementary Fig. S5G), confirming that increased mitophagy resulted in reduced NLRP3 inflammasome activity. Collectively, these data suggested that under the pathological conditions of AD, inhibiting glutamine metabolism in microglia with activated NLRP3 inflammasomes could enhance mitophagy, promote clearance of damaged mitochondria, and reduce intracellular ROS production, ultimately inhibiting inflammasome activity.

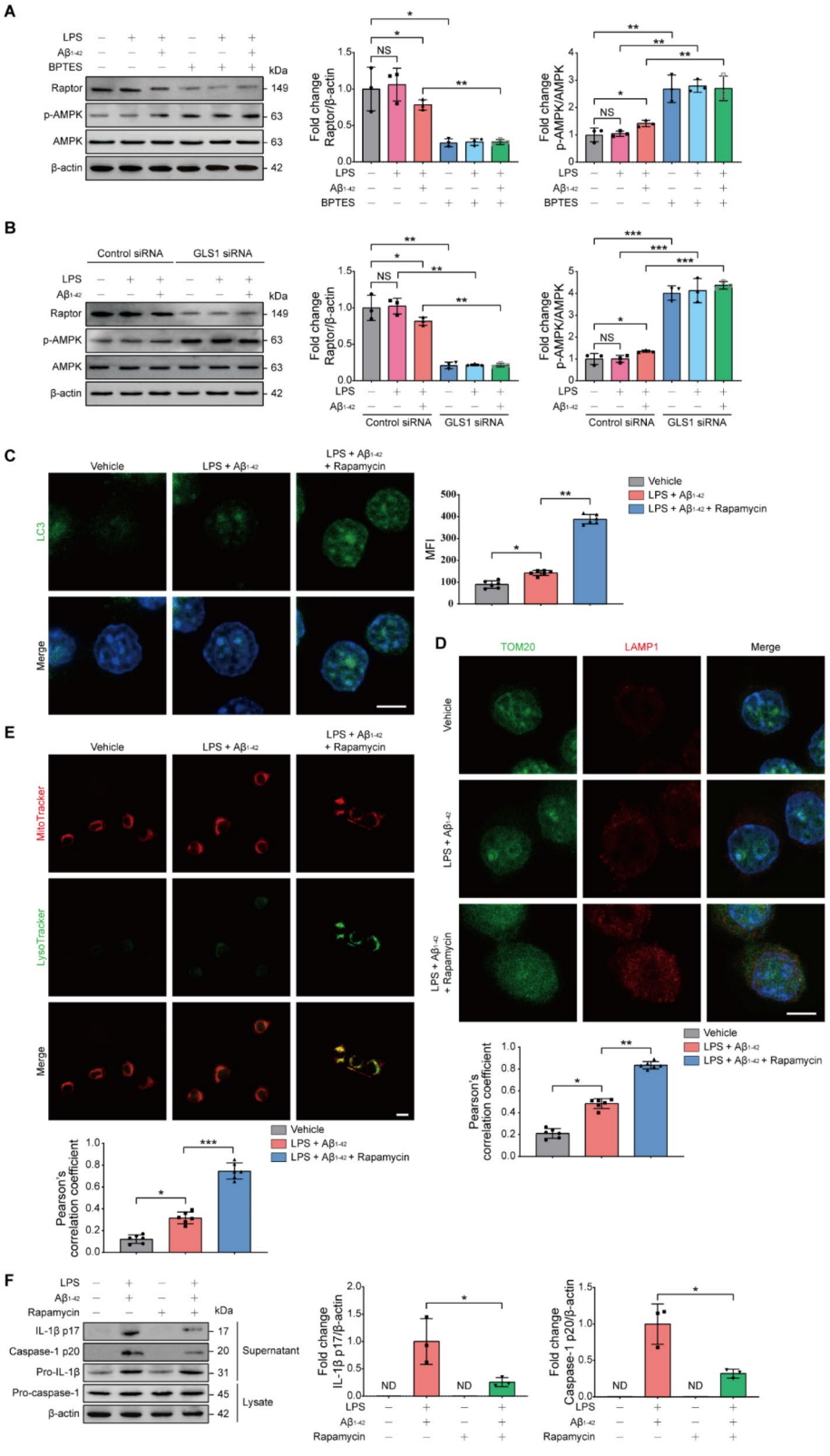

Fig. 6 (See legend on next page.)

(See figure on previous page.)

Fig. 6 Reduced glutamine metabolism enhances mitophagy in LPS-primed oAβ_{1-42}-treated primary microglia via AMPK/mTORC1 signaling. (A and B) WB analysis and densitometry-based quantification of raptor and p-AMPK in LoAMs in the presence or absence of BPTES (**A**) and GLS1 siRNA (**B**) ($n=3$). (**C**) Autophagosome formation indicated by puncta and quantitated by confocal microscopy in LoAMs with or without rapamycin. Scale bar: 10 μm ($n=6$). (**D**) Confocal microscopy detection and quantitation of co-localization of the mitochondrial protein TOM20 (green), lysosomal protein LAMP1 (red), and DAPI (blue) in LoAMs in the presence or absence of rapamycin. Scale bar: 10 μm ($n=6$). (**E**) Confocal microscopy detection and quantitation of co-staining of MitoTracker ang LysoTracker in LoAMs in the presence or absence of rapamycin. Scale bar: 10 μm ($n=6$). (**F**) Western blot analysis of pro- and mature IL-1β and caspase-1 in lysates and supernatants of LoAMs in the presence or absence of rapamycin ($n=3$). ND, not detected. n represents the number of biological replicates. Data are presented as the mean ± SEM. Statistical significance was determined by one-way ANOVA. *$p<0.05$; **$p<0.01$; ***$p<0.001$; NS, not significant

Reduced glutamine metabolism enhances mitophagy in LPS-primed oAβ1–42-treated primary microglia via AMPK/mTORC1 signaling

AMP-activated protein kinase (AMPK) is known to play a major role in the regulation of intracellular energy homeostasis. Specifically, under nutrient deficiency, AMPK is activated to inhibit the function of mammalian target of rapamycin complex 1 (mTORC1), which in turn leads to the induction of autophagy, thereby generating energy for cellular metabolism [39, 40]. Previous work has verified that intracellular glutamine deficiency is accompanied by downregulation of mTORC1 and increased autophagy [41]. Therefore, to determine whether reduced glutamine metabolism also promotes mitophagy, and thus inhibits NLRP3 inflammasome activity via modulation of AMPK/mTORC1 signaling, we analyzed the expression of mTORC1 complex protein Raptor in NLRP3 inflammasome-activated microglia with GLS1 knockdown by BPTES or GLS1-siRNA. Western blots showed that Raptor protein levels were reduced in LoAMs compared to that in vehicle-treated microglia. Moreover, Raptor levels were further decreased in inflammasome-activated microglia with chemical or genetic GLS1 knockdown (Fig. 6A, B). In contrast, LPS and oAβ_{1-42} treatment increased AMPK phosphorylation in microglia, which was further enhanced by GLS1 suppression (Fig. 6A, B). These results suggested that glutamine metabolism could participate in regulating the AMPK/mTORC1 signaling pathway.

To further confirm the relationship between the AMPK/mTORC1 signaling and mitophagy, we inhibited mTORC1 activity with its specific inhibitor, rapamycin, in LPS-primed oAβ_{1-42}-treated microglia and examined the effects on mitophagy-related marker expression. Immunofluorescence staining showed that mTORC1 inhibition by rapamycin increased LC3 expression (Fig. 6C), as well as co-localization of mitochondrial TOM20 with lysosomal LAMP1 (Fig. 6D) and merge staining (yellow) of MitoTracker with LysoTracker (Fig. 6E), compared with that in LPS-primed oAβ_{1-42}-treated primary microglia, indicating that mitophagy was enhanced by mTORC1 inhibition. In addition, we further examined the effects of mTORC1 inhibition on NLRP3 inflammasome activity. Western blot analysis showed that rapamycin treatment led to decreased production of active IL-1β and caspase-1 induced by LPS and oAβ_{1-42} treatment, though not to levels as low as those in vehicle-treated controls (Fig. 6F and Supplementary Fig. S6A), confirming that mTORC1 inhibition results in attenuation of NLRP3 inflammasome activity. Taken together, these results suggested that reducing glutamine metabolism by inhibiting GLS1 could activate AMPK, inhibit mTORC1, and thus promote mitophagy, ultimately blocking NLRP3 inflammasome activity.

Reduced glutamine metabolism enhances mitophagy via AMPK/mTORC1 signaling in microglia of APP/PS1 mice

Given our finding that suppressing glutamine metabolism can ultimately inhibit NLRP3 inflammasome activity by enhancing mitophagy through stimulation of AMPK/inhibition of mTORC1 in LoAMs, we next investigated whether suppressing glutamine metabolism positively regulated mitophagy and AMPK/mTORC1 signaling in microglia of APP/PS1 mice. Western blots showed that expression of mitophagy-related protein p62 was decreased while LC3II levels increased in the $CD11b^+$ microglia of APP/PS1 mice, compared with that in WT mice. In addition, GLS1 inhibition by CB-839 in APP/PS1 mice further decreased p62 expression but increased LC3II accumulation (Fig. 7A). These findings suggested that the microglia of APP/PS1 mice had enhanced mitophagy, and that inhibition of glutamine metabolism further induced mitophagy in order to effectively clear and recycle damaged mitochondria. In agreement with these findings, Raptor levels were reduced while AMPK phosphorylation was increased in the $CD11b^+$ microglia of APP/PS1 mice compared with WT mice, and that suppressing GLS1 expression with CB-839 further reduced raptor accumulation and increased AMPK phosphorylation (Fig. 7A). These findings suggested that inhibition of glutamine metabolism positively regulates AMPK/mTORC1 signaling pathway in microglia of APP/PS1 mice.

Discussion

Microglia-mediated neuroinflammation in AD can function as a metaphorical double-edged sword. Generally, mild neuroinflammation is a function of the host defense against pathogens or host-derived damage signals, whereas excessive inflammation induced by microglia

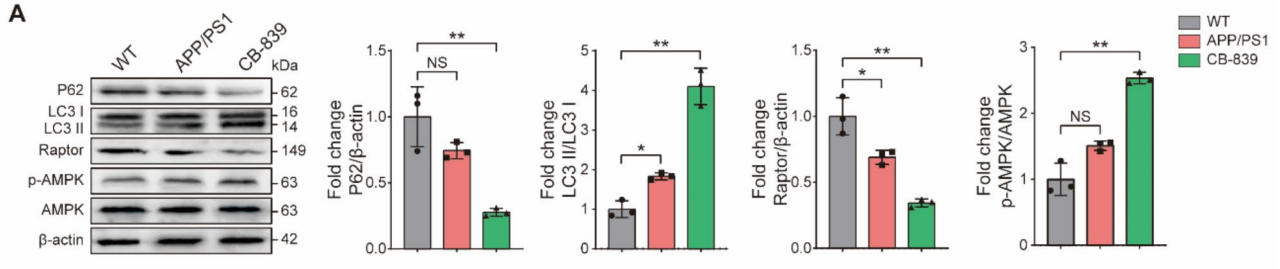

Fig. 7 Reduced glutamine metabolism enhances mitophagy via AMPK/mTORC1 signaling in microglia of APP/PS1 mice. (**A**) WB analysis and quantification of proteins p62, LC3II, raptor and p-AMPK in microglia from 8-month-old female WT mice (gray lines and bars) or APP/PS1 mice in the presence (green lines and bars) or absence (red lines and bars) of CB-839 ($n = 3$). n represents the number of biological replicates. Data are presented as the mean ± SEM. Statistical significance was determined by one-way ANOVA. *$p < 0.05$; **$p < 0.01$; ***$p < 0.001$

can lead to a series of deleterious inflammatory effects and accelerate AD-related neurodegeneration [42]. Therefore, the microglial inflammatory response must be strictly controlled to prevent a pathogenic cascade. The NLRP3 inflammasome protein complexes are key regulators of microglial activation [3]. Studies have shown that NLRP3 inflammasomes play a pivotal role in the pathogenesis of AD [6, 43], but the underlying mechanisms have remained unknown.

Findings of the current study illustrate a pathogenic process/axis in AD disease in which NLRP3 inflammasome activation is accompanied by metabolic reprogramming dominated by glutamine metabolism. Suppression of glutamine metabolism via GLS1 knockdown or inhibition increases the occurrence of mitophagy, reducing intracellular ROS, which thus inhibits activation of NLRP3 inflammasomes and subsequent IL-1β production in microglia. Consistent with the above studies, we observed that administration of GLS1 inhibitor leads to increased mitophagy and decreased NLRP3 inflammasome activity in APP/PS1 mice.

The activation of NLRP3 inflammasomes requires a priming step and an activation step. In the priming stage, cells sense LPS or other pathogen-associated inflammatory response-stimulating factors, which results in transcriptional up-regulation of NLRP3, ASC, and pro-IL-1β. Then host-derived damage-related molecules initiate the activation stage signal pathway to induce the assembly and activation of NLRP3 inflammasomes [31, 44]. Previous studies have found that Aβ can activate NLRP3 inflammasomes by inducing lysosomal disruption [45]. In line with those results, findings in this study show that Aβ has no obvious effect on the priming stage, but can function as a stimulating signal in the activation stage of NLRP3 inflammasomes, consequently inducing an inflammatory response in microglia. In addition, a growing body of evidence supports the likelihood that NLRP3 inflammasome activity is also modulated by intracellular metabolic pathways or endogenous metabolites, especially energy-related metabolism, such as glycolysis, fatty acid metabolism, and the TCA cycle metabolites succinate and itaconate [46]. In this study, untargeted and targeted metabolomics analyses revealed that microglial NLRP3 inflammasomes induced by priming with LPS and activation with $A\beta_{1-42}$ are accompanied by metabolic reprogramming characterized by changes in glutamine metabolism. These findings suggest a strong link between these shifts in glutamine metabolism and activation of NLRP3 inflammasomes by $A\beta_{1-42}$.

Glutamine-related metabolic reprogramming is commonly reported in cancer cells, and has been identified as a mechanism for increasing carbon and nitrogen availability in rapidly proliferating cells [47]. In this process, glutamine-glutamate enters mitochondria where it is converted to α-ketoglutarate (α-KG), which is then transferred to the TCA cycle to produce the reduction equivalents (NADH and $FADH_2$) and intermediate metabolites that ultimately serve as the energy sources and carbon for various biosynthetic processes [28]. Stable isotope tracing analysis in the current study showed that the increased utilization of glutamine following NLRP3 inflammasome activation in microglia is correlated with an increased flux of glutamine-glutamate-α-KG into the TCA cycle and amino acid synthesis. During this anaplerotic process, both oxidative metabolism and reductive carboxylation of glutamine are enhanced, with oxidative metabolism serving as the dominant pathway. Furthermore, our results indicate that microglia produce relatively high concentrations of aspartate and other glutamine-derived amino acids.

In order to further investigate the relationship between glutamine metabolism and NLRP3 inflammasomes, a GLS1 inhibitor and siRNA targeting GLS1 were separately used to suppress glutamine metabolism in microglia. GLS is encoded by two isoenzymes, namely renal glutaminase (KGA/GAC, encoded by *Gls1*) and hepatic glutaminase (LGA/GAB, encoded by *Gls2*) [48]. Previous studies have shown that KGA/GAC is predominantly expressed in the brain, while LGA/GAB expression is negligible and therefore can be ignored [49, 50]. We

used the KGA/GAC small molecule inhibitor, BPTES, and GLS1-siRNA to knock down KGA/GAC expression to down-regulate GLS1 activity in microglia. As a result, we found that secretion of mature caspase-1 and IL-1β decreases under inhibition of intracellular GLS1 after activation of NLRP3 inflammasomes in microglia. In vivo experiments of APP/PS1 mice also demonstrated that administration of the GLS1 inhibitor CB-839 can reduce the activity of NLRP3 inflammasomes and activation of microglia in the brain. Collectively, these findings support a central role for glutamine metabolism in modulating microglial inflammatory response.

The findings in this work demonstrate that inhibiting glutamine metabolism in NLRP3 inflammasome-activated microglia can promote mitophagy through regulation of the AMPK/mTORC1 signaling pathway to clear damaged mitochondria, and thereby reduce intracellular ROS production, ultimately inhibiting NLRP3 inflammasome activity (Fig. 8). It is well known that when mitochondria cannot adapt to nutritional stress caused by metabolic changes, and that mitophagy will occur to clear them to maintain stable mitochondrial function under nutrient deficient conditions [51, 52]. This study shows that microglia adjust their metabolism to adapt to nutritional needs by enhancing glutamine metabolism

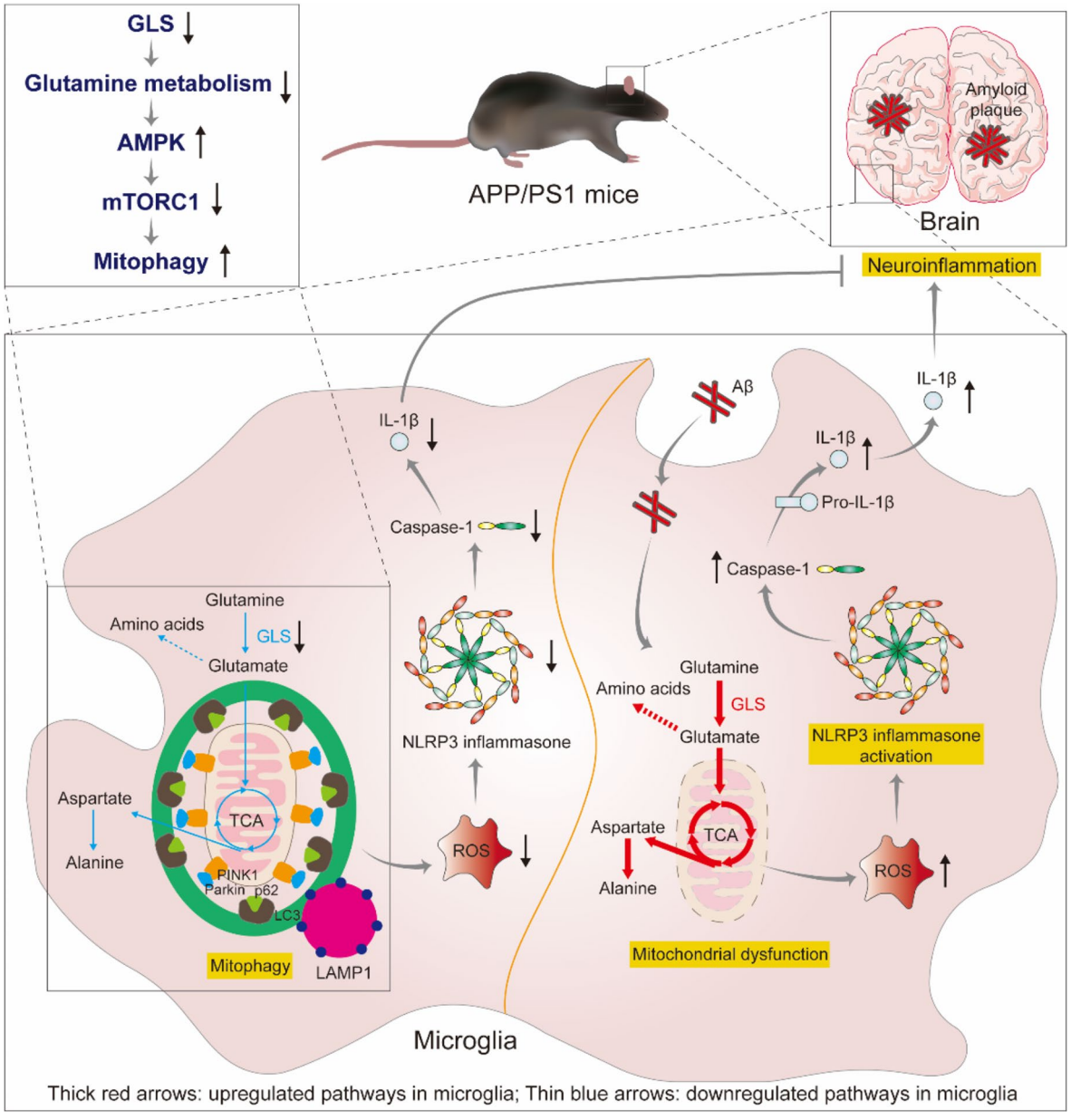

Fig. 8 Graphical abstract of this study

to synthesize a variety of TCA cycle intermediates and amino acids required for phenotypic functional changes during NLRP3 inflammasome activation. Inhibiting GLS1 expression blocks glutamine metabolism, resulting in severe nutrient deficiency in mitochondria, which consequently triggers mitophagy via AMPK/mTORC1 to provide energy for cellular metabolism.

Other studies have shown that mitochondrial dysfunction is linked to various abnormalities of the immune system [53, 54]. Specifically, in cells with defects in mitophagy, damaged mitochondria accumulate, increasing production of mtROS accompanied by the release of intracellular debris, such as mtDNA, into the cytoplasm, which then act as danger signals that can trigger an immune response [55, 56]. Consistent with that scenario, Zhong et al. found that the impaired mitophagic function in macrophages leads to aberrant accumulation of mtDNA and mtROS, followed by activation of NLRP3 inflammasomes which then induce an inflammatory signal cascade, whereas enhanced mitophagy blocks inflammasome activation [13, 57]. Although the relationship between mitophagy and NLRP3 inflammasomes has been confirmed, the specific regulatory mechanism responsible for this series of interactions are still unknown in AD-related neuroinflammation. The results described here bridge this gap in knowledge and illustrate how enhanced mitophagy during the microglial inflammatory response to AD is insufficient to alleviate release of ROS caused by extensive mitochondrial damage. Inhibition of glutamine metabolism can enhance the induction of mitophagy to reduce intracellular ROS and inhibit the activation of NLRP3 inflammasomes, thus supporting glutamine metabolism in microglia as a promising therapeutic target in AD.

Supplementary Information

The online version contains supplementary material available at https://doi.org/10.1186/s12974-024-03254-w.

Supplementary Material 1

Supplementary Material 2

Author contributions

X.Y.G. and Z.X.Z. designed all the experiments. Z.X.Z., Y.W., and X.Y.G. wrote and revised the manuscript. Z.X.Z., M.L., X.L., Z.Y.F. and G.L. carried out the experiments. Z.X.Z. and M.L. collected and analyzed data. All authors reviewed the manuscript.

Funding

This work was financially supported by the National Natural Science Foundation of China (82104364, U21A20407) and the Beijing Natural Science Foundation (7222276).

Data availability

No datasets were generated or analysed during the current study.

Declarations

Ethics approval and consent to participate

All animal experiments were carried out according to the declaration of Helsinki and approved by the ethical committees of Beijing University of Chinese Medicine.

Consent for publication

All the authors consented to the publication of the study once it is accepted.

Competing interests

The authors declare no competing interests.

Received: 10 July 2024 / Accepted: 5 October 2024
Published online: 15 October 2024

References

1. Kwon HS, Koh SH. Neuroinflammation in neurodegenerative disorders: the roles of microglia and astrocytes. Transl Neurodegener. 2020;9:42.
2. Salter MW, Stevens B. Microglia emerge as central players in brain disease. Nat Med. 2017;23:1018–27.
3. Heneka MT, McManus RM, Latz E. Inflammasome signalling in brain function and neurodegenerative disease. Nat Rev Neurosci. 2018;19:610–21.
4. Wang DY, Zhang JB, Jiang WK, Cao ZP, Zhao F, Cai TJ, et al. The role of NLRP3-CASP1 in inflammasome-mediated neuroinflammation and autophagy dysfunction in manganese-induced, hippocampal-dependent impairment of learning and memory ability. Autophagy. 2017;13:914–27.
5. Kuwar R, Rolfe A, Di L, Xu HY, He L, Jiang YQ, et al. A novel small molecular NLRP3 inflammasome inhibitor alleviates neuroinflammatory response following traumatic brain injury. J Neuroinflammation. 2019;16:81.
6. Heneka MT, Kummer MP, Stutz A, Delekate A, Schwartz S, Vieira-Saecker A, et al. NLRP3 is activated in Alzheimer's disease and contributes to pathology in APP/PS1 mice. Nature. 2013;493:674–8.
7. Dempsey C, Rubio Araiz A, Bryson KJ, Finucane O, Larkin C, Mills EL, et al. Inhibiting the NLRP3 inflammasome with MCC950 promotes non-phlogistic clearance of amyloid-β and cognitive function in APP/PS1 mice. Brain Behav Immun. 2017;61:306–16.
8. Zheng D, Liwinski T, Elinav E. Inflammasome activation and regulation: toward a better understanding of complex mechanisms. Cell Discov. 2020;6:36.
9. Shi J, Zhao Y, Wang K, Shi X, Wang Y, Huang H, et al. Cleavage of GSDMD by inflammatory caspases determines pyroptotic cell death. Nature. 2015;526:660–5.
10. Rathinam VA, Fitzgerald KA. Inflammasome complexes: emerging mechanisms and effector functions. Cell. 2016;165:792–800.
11. Ahmed S, Kwatra M, Ranjan Panda S, Murty USN, Naidu VGM. Andrographolide suppresses NLRP3 inflammasome activation in microglia through induction of parkin-mediated mitophagy in in-vitro and in-vivo models of Parkinson disease. Brain Behav Immun. 2021;91:142–58.
12. Kim MJ, Yoon JH, Ryu JH. Mitophagy: a balance regulator of NLRP3 inflammasome activation. BMB Rep. 2016;49:529–35.
13. Zhong Z, Umemura A, Sanchez-Lopez E, Liang S, Shalapour S, Wong J, et al. NF-κB restricts inflammasome activation via elimination of damaged mitochondria. Cell. 2016;164:896–910.
14. Annesley SJ, Fisher PR. Mitochondria in health and disease. Cells. 2019;8:680.
15. Baik SH, Kang S, Lee W, Choi H, Chung S, Kim JI, et al. A breakdown in metabolic reprogramming causes microglia dysfunction in Alzheimer's disease. Cell Metab. 2019;30:493–507.
16. Pan RY, He L, Zhang J, Liu X, Liao Y, Gao J, et al. Positive feedback regulation of microglial glucose metabolism by histone H4 lysine 12 lactylation in Alzheimer's disease. Cell Metab. 2022;34:634–48.
17. Johnson ECB, Dammer EB, Duong D, Ping L, Zhou M, Yin L, et al. Large-scale proteomic analysis of Alzheimer's disease brain and cerebrospinal fluid reveals early changes in energy metabolism associated with microglia and astrocyte activation. Nat Med. 2020;26:769–80.
18. Li Y, Zheng JY, Liu JQ, Yang J, Liu Y, Wang C, et al. Succinate/NLRP3 inflammasome induces synovial fibroblast activation: therapeutical effects of clematichinenoside AR on arthritis. Front Immunol. 2016;7:532.
19. Liu Y, Xu RY, Gu HY, Zhang EF, Qu JW, Cao W, et al. Metabolic reprogramming in macrophage responses. Biomark Res. 2021;9:1.

20. Karasawa T, Kawashima A, Usui-Kawanishi F, Watanabe S, Kimura H, Kamata R, et al. Saturated fatty acids undergo intracellular crystallization and activate the NLRP3 inflammasome in macrophages. Arterioscler Thromb Vasc Biol. 2018;38:744–56.
21. Moon JS, Nakahira K, Chung KP, DeNicola GM, Koo MJ, Pabón MA, et al. NOX4-dependent fatty acid oxidation promotes NLRP3 inflammasome activation in macrophages. Nat Med. 2016;22:1002–12.
22. Guo CS, Xie SJ, Chi ZX, Zhang JH, Liu YY, Zhang L, et al. Bile acids control inflammation and metabolic disorder through inhibition of NLRP3 inflammasome. Immunity. 2016;45:802–16.
23. Sokolowska M, Chen LY, Liu Y, Martinez-Anton A, Qi HY, Logun C, et al. Prostaglandin E2 inhibits NLRP3 inflammasome activation through EP4 receptor and intracellular cyclic AMP in human macrophages. J Immunol. 2015;194:5472–87.
24. Moon JS, Hisata S, Park MA, DeNicola GM, Ryter SW, Nakahira K, et al. mTORC1-induced HK1-dependent glycolysis regulates NLRP3 inflammasome activation. Cell Rep. 2015;12:102–15.
25. Xie M, Yu Y, Kang R, Zhu S, Yang LC, Zeng L, et al. PKM2-dependent glycolysis promotes NLRP3 and AIM2 inflammasome activation. Nat Commun. 2016;7:13280.
26. Stein WH, Moore S. The free amino acids of human blood plasma. J Biol Chem. 1954;211:915–26.
27. DeBerardinis RJ, Mancuso A, Daikhin E, Nissim I, Yudkoff M, Wehrli S, et al. Beyond aerobic glycolysis: transformed cells can engage in glutamine metabolism that exceeds the requirement for protein and nucleotide synthesis. Proc Natl Acad Sci USA. 2007;104:19345–50.
28. Le A, Lane AN, Hamaker M, Bose S, Gouw A, Barbi J, et al. Glucose-independent glutamine metabolism via TCA cycling for proliferation and survival in B cells. Cell Metab. 2012;15:110–21.
29. Tannahill GM, Curtis AM, Adamik J, Palsson-McDermott EM, McGettrick AF, Goel G, et al. Succinate is an inflammatory signal that induces IL-1β through HIF-1α. Nature. 2013;496:238–42.
30. Halle A, Hornung V, Petzold GC, Stewart CR, Monks BG, Reinheckel T, et al. The NALP3 inflammasome is involved in the innate immune response to amyloid-beta. Nat Immunol. 2008;1636:857–65.
31. Bauernfeind FG, Horvath G, Stutz A, Alnemri ES, MacDonald K, Speert D, et al. Cutting edge: NF-kappaB activating pattern recognition and cytokine receptors license NLRP3 inflammasome activation by regulating NLRP3 expression. J Immunol. 2009;183:787–91.
32. Man SM, Kanneganti TD. Regulation of inflammasome activation. Immunol Rev. 2015;265:6–21.
33. Iyer SS, He Q, Janczy JR, Elliott EI, Zhong Z, Olivier AK, et al. Mitochondrial cardiolipin is required for Nlrp3 inflammasome activation. Immunity. 2013;39:311–23.
34. Groß CJ, Mishra R, Schneider KS, Médard G, Wettmarshausen J, Dittlein DC, et al. K^+ efflux-independent NLRP3 inflammasome activation by small molecules targeting mitochondria. Immunity. 2016;45:761–73.
35. Thangavelu K, Pan CQ, Karlberg T, Balaji G, Uttamchandani M, Suresh V, et al. Structural basis for the allosteric inhibitory mechanism of human kidney-type glutaminase (KGA) and its regulation by Raf-Mek-Erk signaling in cancer cell metabolism. Proc Natl Acad Sci USA. 2012;109:7705–10.
36. Gross MI, Demo SD, Dennison JB, Chen L, Chernov-Rogan T, Goyal B, et al. Antitumor activity of the glutaminase inhibitor CB-839 in triple-negative breast cancer. Mol Cancer Ther. 2014;13:890–901.
37. Sena LA, Chandel NS. Physiological roles of mitochondrial reactive oxygen species. Mol Cell. 2012;48:158–67.
38. Galluzzi L, Baehrecke EH, Ballabio A, Boya P, Bravo-San Pedro JM, Cecconi F, et al. Molecular definitions of autophagy and related processes. EMBO J. 2017;36:1811–36.
39. Hardie DG. AMPK and autophagy get connected. EMBO J. 2011;30:634–5.
40. Tan VP, Miyamoto S. Nutrient-sensing mTORC1: integration of metabolic and autophagic signals. J Mol Cell Cardiol. 2016;95:31–41.
41. Tan HWS, Sim AYL, Long YC. Glutamine metabolism regulates autophagy-dependent mTORC1 reactivation during amino acid starvation. Nat Commun. 2017;8:338.
42. Cunningham C. Microglia and neurodegeneration: the role of systemic inflammation. Glia. 2013;61:71–90.
43. Tan MS, Yu JT, Jiang T, Zhu XC, Tan L. The NLRP3 inflammasome in Alzheimer's disease. Mol Neurobiol. 2013;48:875–82.
44. Sutterwala FS, Haasken S, Cassel SL. Mechanism of NLRP3 inflammasome activation. Ann N Y Acad Sci. 2014;1319:82–95.
45. He Y, Hara H, Núñez G. Mechanism and regulation of NLRP3 inflammasome activation. Trends Biochem Sci. 2016;41:1012–21.
46. Hughes MM, O'Neill L. Metabolic regulation of NLRP3. Immunol Rev. 2018;281:88–98.
47. Wise DR, Thompson CB. Glutamine addiction: a new therapeutic target in cancer. Trends Bio Sci. 2010;35:427–33.
48. Elgadi KM, Meguid RA, Qian M, Souba WW, Abcouwer SF. Cloning and analysis of unique human glutaminase isoforms generated by tissue-specific alternative splicing. Physiol Genomics. 1999;1:51–62.
49. van den Heuvel AP, Jing J, Wooster RF, Bachman KE. Analysis of glutamine dependency in non-small cell lung cancer: GLS1 splice variant GAC is essential for cancer cell growth. Cancer Biol Ther. 2012;13:1185–94.
50. Cassago A, Ferreira AP, Ferreira IM, Fornezari C, Gomes ER, Greene KS, et al. Mitochondrial localization and structure-based phosphate activation mechanism of glutaminase C with implications for cancer metabolism. Proc Natl Acad Sci USA. 2012;109:1092–7.
51. Suliman HB, Piantadosi CA. Mitochondrial quality control as a therapeutic target. Pharmacol Rev. 2016;68:20–48.
52. Yang X, Zhang RY, Nakahira K, Gu ZL. Mitochondrial DNA mutation, diseases, and Nutrient-Regulated Mitophagy. Annu Rev Nutr. 2019;39:201–26.
53. West AP, Shadel GS, Ghosh S. Mitochondria in innate immune responses. Nat Rev Immunol. 2011;11:389–402.
54. Wenceslau CF, McCarthy CG, Szasz T, Spitler K, Goulopoulou S, Webb RC. Mitochondrial damage-associated molecular patterns and vascular function. Eur Heart J. 2014;35:1172–7.
55. West AP, Shadel GS. Mitochondrial DNA in innate immune responses and inflammatory pathology. Nat Rev Immunol. 2017;17:363–75.
56. Kanneganti TD, Kundu M, Green DR. Innate immune recognition of mtDNA-an undercover signal? Cell Metab. 2015;21:793–4.
57. Zhong Z, Liang S, Sanchez-Lopez E, He F, Shalapour S, Lin XJ, et al. New mitochondrial DNA synthesis enables NLRP3 inflammasome activation. Nature. 2018;560:198–203.

Publisher's note